Characteristics of Two Types of Chloride Channel in Sarcoplasmic Reticulum Vesicles from Rabbit Skeletal Muscle

Joseph I. Kourie, Derek R. Laver, Pauline R. Junankar, Peter W. Gage, and Angela F. Dulhunty
John Curtin School of Medical Research, Australian National University, Canberra City, ACT 2601, Australia

ABSTRACT A comparison is made of two types of chloride-selective channel in skeletal muscle sarcoplasmic reticulum (SR) vesicles incorporated into lipid bilayers. The I/V relationships of both channels, in 250/50 mM Cl^- (*cis/trans*), were linear between −20 and +60 mV (*cis* potential,) reversed near E_{Cl} and had slope conductances of ~250 pS for the big chloride (BCl) channel and ~70 pS for the novel, small chloride (SCl) channel. The protein composition of vesicles indicated that both channels originated from longitudinal SR and terminal cisternae. BCl and SCl channels responded differently to *cis* SO_4^{2-} (30–70 mM), 4,4′-diisothiocyanatostilbene 2,2′-disulfonic acid (8–80 μM) and to bilayer potential. The BCl channel open probability was high at all potentials, whereas SCl channels exhibited time-dependent activation and inactivation at negative potentials and deactivation at positive potentials. The duration and frequency of SCl channel openings were minimal at positive potentials and maximal at −40 mV, and were stationary during periods of activity. A substate analysis was performed using the Hidden Markov Model (S. H. Chung, J. B. Moore, L. Xia, L. S. Premkumar, and P. W. Gage, 1990, *Phil. Trans. R. Soc. Lond. B.*, 329:265–285) and the algorithm EVPROC (evaluated here). SCl channels exhibited transitions between 5 and 7 conductance levels. BCl channels had 7–13 predominant levels plus many more short-lived substates. SCl channels have not been described in previous reports of Cl^- channels in skeletal muscle SR.

INTRODUCTION

The sarcoplasmic reticulum (SR) of skeletal muscle is responsible for accumulation, storage, and release of the calcium ions that initiate contraction. The SR membrane contains at least three classes of ion channel: ryanodine receptor Ca^{2+} release channels, K^+ channels, and Cl^- channels. The Ca^{2+} release channel is directly involved in excitation-contraction coupling and has been subjected to intense investigation (see, e.g., Smith et al., 1985). The K^+ channel has also been studied in considerable detail (Miller and Racker, 1976; Miller, 1978; Coronado et al., 1980; Wang and Best, 1994). Cl^- channels from SR membranes have been described (Table 1) but not characterized in detail, even though they are likely to mediate part of the countercurrent that stabilizes SR membrane potential during large transmembrane movements of Ca^{2+} ions.

Several types of Cl^- channels incorporated into lipid bilayers, or liposomes, from SR vesicles exhibit voltage-independent gating (Table 1, nos. 1–7), but differ in their conductance, selectivity, and sensitivity to blocking agents. The 200 pS channel reported by Tanifuji et al. (1987) has a high open probability (P_o) and, like the 70 pS Cl^- channel identified by Rousseau et al. (1988), is anion-selective and has flickering activity with four or five different subconductance states. Sukhareva et al. (1994) found a nonselective Cl^- channel with high Ca^{2+} permeability that is blocked by ruthenium red. Ide et al. (1991) purified a 100 kDa protein from longitudinal SR vesicles, which produced Cl^- channels in lipid bilayers. In contrast to P_o of channels in skeletal SR vesicles, P_o in a channel from cardiac SR has some voltage-dependent gating properties, although voltage-dependent activation and inactivation are not observed (Table 1, no. 8).

Skeletal SR anion channels have also been observed in patch clamp studies of extruded blebs of SR (Table 1 nos. 9–10). These channels differ from those seen in bilayers in that they have a bell-shaped dependence of P_o on voltage, and much higher Cl^- conductances.

Cl^- channels seen in patch clamp studies of skeletal sarcolemma differ from Cl^- channels seen when SR vesicles are incorporated into bilayers in that P_o in the sarcolemmal channels is voltage-dependent (Table 1, nos. 11–12 and 14–17). Cl^- channels are rarely seen in patch clamp studies of mammalian sarcolemma, presumably because in contrast to amphibia most of the Cl^- conductance is in the T-tubule membrane (Eisenberg and Gage, 1969; Palade and Barchi, 1977; Dulhunty, 1979). Chua and Betz (1991) recorded only three instances of Cl^- channels in 139 patches of sarcolemma from rat skeletal muscle (Table 1, no. 14). These channels were similar to a channel commonly seen on the surface of cultured rat myocytes (Table 1, no. 16), which showed long openings at all membrane potentials and a higher P_o at potentials positive to the resting membrane potential. Blatz and Magleby (1983, 1985; Table 1, nos. 11 and 15) found two additional types of sarcolemmal Cl^- channel in cultured myocytes: a high conductance channel that is spontaneously active at 0 mV but closes to an inactivated state with steps to either positive or negative membrane potentials, and a low conductance channel with fast kinetics and openings at the resting potential (−80 mV). A high conductance, voltage-dependent Cl^- channel has

---

Received for publication 23 December 1994 and in final form 18 October 1995.

Address reprint requests to Dr. J. I. Kourie, JCSMR, P.O. Box 334, Canberra City, ACT 2601, Australia. Tel.: 06-249-2758; Fax: 06-249-47611; E-mail: joseph.kourie@anu.edu.au.

0006-3495/96/01/202/20 $2.00

TABLE 1 Properties of muscle Cl^- channels

Channel no.	Membrane type*	Conductance (γ) (pS)	([Cl]) *cis/trans* (mM)	V_{Po}[‡]	$V_{A/I}$[§]	Method	Species	Source manuscripts
Large conductance SR channels								
1	Crude SSR	200	100/100	−	−/−	Bilayer	Rabbit	Tanifuji et al. (1987)
2	HSSR	290	355/55	−	−/−	Bilayer	Rabbit	Hamilton et al. (1989)
3	HSSR & LSSR	200	450/50	−	−/−	Bilayer	Rabbit	Sukhareva et al. (1994)
4	HSSR	490	150/150	−	−/−	Patch/LSV[¶]	Rabbit	Hals et al. (1989)
Small conductance SR channels								
5, 6	HSSR & LSSR	115	300/100	−	−/−	Bilayer	Rabbit	Rousseau et al. (1988), Smith et al. (1986)
7	HSSR & LSSR	70	125/125	−	−/−	Bilayer	Rabbit	Ide et al. (1991)
8	CSR-bands 1 to 5	55	250/60	+	−/−	Bilayer	Dog	Rousseau (1989)
Channels in sarcoballs								
9, 10	SSR-blebs	600	200/200	+	−/+	Patch	Frog	Lewis et al. (1992), Hals et al. (1989)
Large conductance channels on sarcolemma								
11	CMS	440	143/143	+	−/+	Patch	Rat	Blatz and Magleby (1983)
12	SS	280	110/110	+	−/−	Patch	Frog	Woll and Neumcke (1987)
13	SS	200–280	140/140	−	−/−	Patch/LSV	Mouse	Wischmeyer et al. (1995)
Small conductance channels on sarcolemma								
14	SS	60	141/141	+	−/−	Patch	Rat	Chua and Betz (1991)
15, 16	CMS	45–61	100/100	+	−/−	Patch	Rat	Blatz and Magleby (1985),
17		1	135/140	+	−/−	Patch	HEK295	Pusch et al. (1994)
18	SS	35–150	140/140	−	−/−	Patch/LSV	Mouse	Wischmeyer et al. (1995)
T-tubule channels								
19	TT	40	300/100	−	−/−	Bilayer	Rabbit	Hidaka et al. (1993)
SCl	LSSR & HSSR	250	250/50	−	−/−	Bilayer	Rabbit	
BCl	LSSR & HSSR	75	250/50	+	+/+	Bilayer	Rabbit	

*Membrane type: HSSR & LSSR, heavy and light skeletal SR; CSR, cardiac SR; SS, skeletal sarcolemma; CSMS, cultured skeletal myocyte sarcolemma; TT, T-tubule.

[‡] Open probability (P_o) is (+), is not (−), voltage-dependent (V_{Po}).

[§] Activation/inactivation are (+), are not (−), voltage-dependent ($V_{A/I}$).

[¶] LSV, lipid supplemented vesicles.

also been recorded in the plasmalemma of amphibian skeletal muscle (Table 1, no. 12): P_o in this channel is near 1 at potentials between −40 and +80 mV, but <0.1 between −40 mV and −80 mV. A preliminary patch clamp study of plasmalemma channels incorporated into lipid supplemented vesicles (Table 1, nos. 13 and 18) demonstrated five channel types with different conductances (presumably Cl^-) and with gating characteristics similar to many of the plasmalemma chloride channels previously described.

The ClC-1 protein expressed in HEK293 cells supports a voltage-dependent Cl^- current; noise analysis of the current suggests a single channel conductance of ~1 pS (Table 1, no. 17). ClC-1 is located in plasmalemma but not in T-tubules (Gurnett et al., 1995) and is unlikely to underlie the macroscopic Cl^- conductance in the T-tubule membrane (above), although it has been suggested that the ClC-1 protein forms the major chloride channel in the surface membrane of skeletal muscle.

A channel from the T-tubule membrane has been studied in lipid bilayers (Table 1, no. 19). It has a smaller single channel conductance than channels reported from SR and plasmalemma, and its P_o is independent of voltage.

Although several types of anion channel have been described in skeletal SR vesicles (above), previous studies have not attempted to directly compare the different channels or to study their gating characteristics in detail. The aim of the present study was 1) to compare the distribution, conductance, voltage-dependence and sensitivity to SO_4^{2-} and 4,4′-diisothiocyanatostilbene 2,2′-disulfonic acid (DIDS) of two anion channels in skeletal SR vesicles and 2) to provide a detailed study of the gating characteristics and subconductance activity. The larger or "big" conductance channel (called BCl, by analogy with B-K channels) is similar to the channel described by Tanifuji et al. (1987); the other smaller channel (small Cl^- channel, SCl) has characteristics that differ in several significant ways from those of any skeletal muscle SR, plasmalemma, or T-tubule anion channel described previously (Table 1). The SCl channel demonstrates unique voltage-dependent activation and inactivation characteristics and appears to be a novel Cl^- channel.

A problem faced in all bilayer studies using SR vesicles is that membrane preparations are contaminated to some extent with T-tubule membrane and sarcolemma (e.g., Mitchell et al., 1983) and channels in these contaminant membranes may also appear in bilayers. Frequently observed channels in SR vesicles (Table 1, nos. 1–8) are generally believed to originate from the SR membranes, because most vesicles are of SR origin and because the characteristics of the channels differ from those seen in sarcolemma and T-tubule membranes. In addition to these qualitative arguments we provide quantitative evidence that the BCl and SCl channels that we observe are of SR origin.

Some of the results have been reported previously (Kourie et al., 1992).

MATERIALS AND METHODS

Preparation of SR vesicles

SR vesicle fractions (bands 1 to 4) were prepared using methods based on those of Saito et al. (1984) and have been described previously (Ahern et al., 1994; Laver et al., 1995).

Electrophoresis and Western blots

Aliquots of each SR band were subjected to electrophoresis on either a 5–17% or 3–12% sodium dodecyl sulfate (SDS)-polyacrylamide gradient gel (Junankar et al., 1995). Western blots onto Immobilon membranes (Millipore, Boston, MA) were carried out at 4°C in a BioRad (Richmond, CA) Mini Trans-blot Cell using 10 mM 2-[*N*-cyclohexylamino]ethanesulfonic acid, pH 9.6, containing 10% ethanol and 0.05% SDS as the buffer system (ethanol/SDS were omitted when the blot was stained for the dihydropyridine receptor (DHPR)). The blots were blocked with 5% skim milk powder in 20 mM Tris, 500 mM NaCl, pH 7.5 (TBS) before incubating with primary antibodies overnight at 4°C. The antibodies used were 1) anti-skeletal Ca^{2+},Mg^{2+}-ATPase, D12 (Dulhunty et al., 1987); 2) anti-skeletal ryanodine receptor, 5C3 (Dulhunty et al., 1992); 3) anti-skeletal α1-subunit of DHPR, mAb1 (Morton and Froehner, 1987); and 4) anti-dystrophin (MANDYS 8, Sigma Chemical Co., St. Louis, MO). The secondary antibody was either anti-mouse IgG alkaline phosphatase (1:5000 dilution in TBS containing 0.1% Tween-20) described in Dulhunty et al., 1987, or horseradish peroxidase conjugate (1:2000 dilution) visualized using the enhanced chemiluminescence kit (Amersham, Arlington Heights, IL) following manufacturer's instructions.

Bilayer cups, lipid bilayers, and vesicle fusion

Bilayers were formed across 150 μm apertures from a mixture of palmitoyl-oleoyl-phosphatidylethanolamine, palmitoyl-oleoyl-phosphatidylserine, and palmitoyl-oleoyl-phosphatidylcholine (5:3:2, by volume; Ahern et al., 1994; Laver et al., 1995). The formation of the lipid bilayer from the thick lipid film was detected from its total capacitance, which increased to values of 150 pF to 170 pF during thinning. The membrane capacitance was measured from the current response to a voltage ramp ranging from 0 to −140 mV in 140 ms (1 V/s, the "bilayer test"; see Kourie, 1995). SR vesicles were added to a final protein concentration of 1–10 μg/ml and the solution stirred vigorously until the appearance of channel activity indicated vesicle fusion. The side of the bilayer to which vesicles were added was defined as *cis*, and the other side as *trans*. It was assumed that the cytoplasmic side of the SR membrane faced the *cis* chamber (Miller and Racker, 1976); this was confirmed in our B4 vesicles where the sensitivity of the ryanodine receptor to ligands, which are known to bind to the cytoplasmic domain of the protein, was tested (Ahern et al., 1994; Laver et al., 1995).

Solutions for bilayers

Solutions contained choline Cl (250 mM *cis*/50 mM *trans*) or CsCl (250, 150, or 100 mM *cis*/50 mM *trans*), plus 1 mM $CaCl_2$ and 10 mM HEPES (pH 7.2, adjusted with NaOH). When solutions contained SO_4^{2-} or DIDS, appropriate volumes of 100 mM Li_2SO_4 or 12.5 mM (or 125 mM) DIDS were added to the solutions in the bilayer chamber.

Recording single channel activity

Voltage was controlled and current recorded as described previously (Ahern et al., 1994; Laver et al., 1995). Potentials are given with respect to the *trans* chamber. For analysis, current was filtered at 1 kHz (−3 dB, 4-pole bessel) and digitized with a TL-1 DMA interface (Labmaster, Axon Instruments, Foster City, CA) at 2 kHz. Experiments were done at 20–25°C.

When bilayers contained the BCl channel, there was clearly a conductance in parallel with the bilayer capacitance. From the "bilayer test" it could not be determined whether this shunt was via the ion channel or through a nonspecific bilayer leak. To avoid contamination of BCl currents by any leak current, the analyses of BCl channel activity described here were done on currents recorded at 0 mV, at which potential the contribution from nonspecific leak currents would be minimal. Our criteria for defining ion currents as belonging to a "single channel" are outlined in the Discussion.

Analysis of single channel data

Three different analysis programs were used to investigate different aspects of single channel activity.

CHANNEL2

An in-house analysis program (developed by P. W. Gage and M. Smith), was used to measure the following parameters of channel activity: open time, T_o; frequency of opening, F_o; closed time, T_c; the sum of all open times as a fraction of the total time, i.e., open probability, P_o; the integral of the current divided by the total time, i.e., the mean current, I'. Open times were defined as intervals where the current exceeded the baseline noise. Records were filtered for CHANNEL2 analysis using a running average of three to five data points, and the threshold for channel opening or closing was normally set between −0.4 and −0.6 pA.

Hidden Markov Model and EVPROC

Current levels were extracted from background noise either by using the Hidden Markov Model (HMM) (Chung et al., 1990; Gage and Chung, 1994), or by a transition detection method (EVPROC, developed by D. R. Laver). The HMM analysis is based on the assumption that a recorded signal represents the sum of Gaussian noise of known variance and a first-order, finite-state, homogeneous Markov process. The parameters of this model are systematically adjusted to obtain the most likely signal that fits the data. The HMM technique gives *a posteriori* estimates of the most likely signal statistics, including the Markov model state transition probabilities, open and closed time probabilities, and signal levels. It has been shown that small known signals buried in Gaussian noise can be accurately extracted using this technique (Chung et al., 1990; Gage and Chung, 1994). HMM uses several subroutines to obtain the signal properties. The first (routine A) evaluates the most likely amplitude histogram of the underlying signal. Routine B determines the most likely level amplitudes for a given number of levels. Routine C then uses the levels obtained with routine B to model the signal sequence and conductance levels of the channel, giving an idealized signal in the absence of noise. HMM provides a powerful method for defining conductance states and kinetics of channel currents. However, the computations require large amounts of computer time so that only short segments of data can be readily analyzed. A full description and evaluation of HMM is given in Chung et al. (1990).

EVPROC (see Appendix) provides a faster method that assumes that the underlying signal is a series of stepwise transitions. The raw data are initially reduced to a series of putative stationary levels (Vivaudou et al., 1986), and the transitions between the levels are then tested for significance. A transition step, T, is significant when:

$$(T/\sqrt{n}) > 2I_{\mathrm{RMS}} \tag{1}$$

where n is a minimum number of samples in the levels adjoining the transition. I_{RMS} is the root mean square of the noise, obtained from sections of the record that do not contain ion channel currents. Transitions that are not significant are removed by replacing the adjacent levels with their weighted mean. The resulting levels are tested and the procedure continued until all transitions meet the above criteria. The amplitude histograms, mean durations, and transition frequencies from the EVPROC analysis are obtained directly from the idealized signal generated by EVPROC. The mean durations were calculated from EVPROC by dividing the total number of data samples by the number of events at a given amplitude. The pattern of transitions between conductance states is shown by two-dimensional, cartesian intensity plots. The reliability of EVPROC is assessed in the Appendix (below).

The basic difference between HMM and EVPROC is that HMM iteratively evaluates the whole record for the most likely levels according to the most probable transition matrix of the underlying Markov signal. In contrast, EVPROC directly notes all levels (within the limits of the noise) and produces a distribution of levels.

The best resolution of peaks within the amplitude histograms produced by the two techniques was obtained when the raw data were low-pass filtered at 1 kHz. This is probably because the noise on the bilayer current increased with frequency above 1 KHz.

Both HMM and EVPROC provided analyses of current transitions. The kinetics of current transitions can be summarized by a matrix of transition probabilities, P_{ij}, which gives the probability that the signal in state "i" steps to state "j" during the sample interval, dt. The gating kinetics could be more clearly illustrated in histograms showing the mean duration of each current level and in diagrams of the relative frequency of transitions to the other levels. In the HMM analysis, the mean duration, t_i, of level i was calculated from the diagonal elements of the transition matrix P_{ii} using the equation $t_i = -dt/\ln[P_{ii}]$. The relative transition frequencies F_{ij} between states i and j could also be derived from transition matrix and the level probabilities, p_i, by the equation

$$F_{ij} = A.P_{ij}.p_i/(t_i(1 - P_{ii})) \tag{2}$$

where A is a scaling factor that depends on the total number of transitions in the record. In the EVPROC analysis the mean durations were calculated by dividing the total number of data samples by the number of events at a given amplitude.

The EVPROC analysis program can be requested from Dr. D. R. Laver.

RESULTS

Protein composition of SR vesicles

SDS-polyacrylamide gels of bands 1–4, stained with Coomassie blue (not shown), showed a profile similar to that obtained by Saito et al. (1984). Western blots of the gels (Fig. 1 *A*) were used to confirm the presence of the 560 kDa ryanodine receptor; the 105 kDa SR Ca^{2+},Mg^{2+}-ATPase; the 180 kDa $\alpha 1$ subunit of the DHPR; and the 429 kDa dystrophin. Band 4 contained most of the high molecular weight ryanodine receptor and a ~60 kDa band (on Coomassie blue-stained gels) corresponding to calsequestrin. The presence of the ryanodine receptor and the 60 kDa band indicated that band 4 is highly enriched in terminal cisternae membranes. The major protein in all SR vesicle fractions was the Ca^{2+},Mg^{2+}-ATPase at 110 kDa. Smaller amounts of the ryanodine receptor were also located in band 3, which is thought to contain a mixture of terminal cisternae and longitudinal SR. Bands 1 and 2 contained very little ryanodine receptor. Dystrophin, which is mostly associated with the plasma membrane, was detected in band 1, but could not be detected in the other bands.

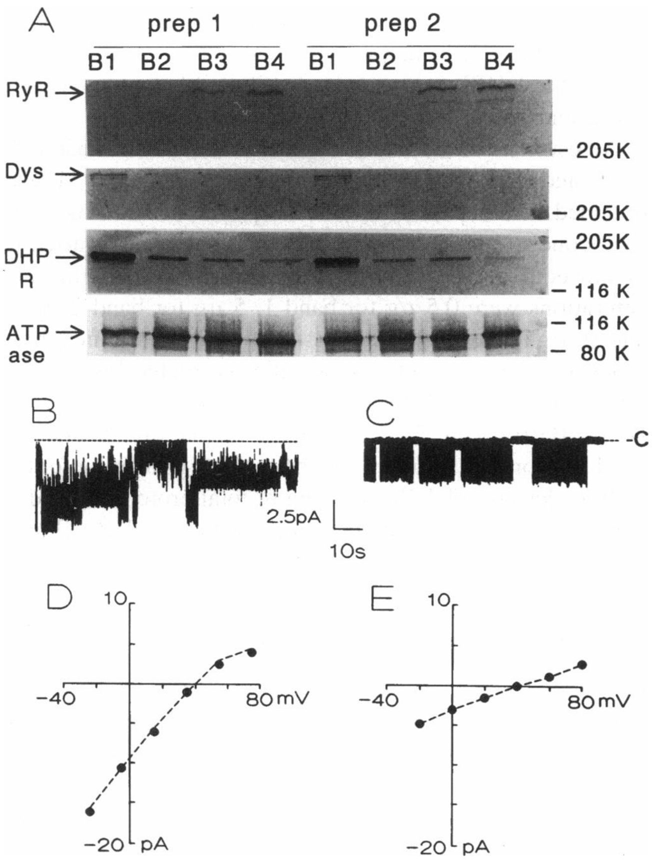

FIGURE 1 (*A*) Western blots of proteins in vesicles from bands 1, 2, 3, and 4 (B1, B2, B3, and B4) from two different SR preparations (prep 1 and prep 2). The antibodies used are listed in Materials and Methods. The first panel shows immunostaining of the ryanodine receptor (terminal cisternae marker) mostly in B4, with some activity in B3. The second panel shows immunostaining of dystrophin (sarcolemma marker) only in B1. The third panel shows immunostaining of the DHPR (T-tubule marker) mostly in B1, with progressively lower densities in B2–B4. The fourth panel shows immunostaining of the Ca-ATPase (longitudinal SR and terminal cisternae marker) in all bands. Prestained molecular weight markers (BioRad) are shown. The position and weight of the markers are indicated on the right side of *A*. The total protein added was the same for each band and was 1 μg for RyR and Ca-ATPase staining (panels 1 and 4) and 5 μg for dystrophin and DHPR staining (panels 2 and 3). *B* and *C* show, respectively, records of single BCl and SCl channels recorded at 0 mV. The dotted lines indicate the closed levels for the channels. The record in C is atypical in that it has been selected to show events in which the channel is fully closed. *D* and *E* show current-voltage relationships for the channels in *A* and *B*. Filled circles show the maximum current recorded at each voltage. The unitary conductances are 245 pS for the BCl channel and 75 pS for the SCl channel. Dotted lines have been drawn by eye through the data points. Voltage is expressed as the potential in the *cis* chamber with respect to the *trans* chamber.

The T-tubule marker, the DHPR, was most concentrated in band 1, less concentrated in band 2, and just detectable in bands 3 and 4 in the two preparations illustrated in Fig. 1 *A*.

A similar pattern of staining was found in two other preparations. In a fifth, atypical, preparation (Junankar et al., 1995), the DHPR was evenly distributed between bands 1 and 2 and absent from bands 3 and 4.

An estimate of the relative amounts of DHPR in bands 1, 2, 3, and 4 in the preparations shown in Fig. 1 *A* was obtained in a separate series of experiments in which the total concentrations of protein in each band were varied to obtain equivalent staining on Western blots. Protein concentrations were 0.5 μg for band 1, 5 μg for band 2 and 3 and 10 μg for band 4. The Western blots were scanned three times and the mean relative densities corrected for concentration differences. The relative concentration of DHPR in B1:B2:B3:B4 were 22:2.2:2.1:1 for preparation 1, and 12: 1.5:1.6:1 for preparation 2. MAb1 had a high affinity for the DHPR, detecting DHPR in 10 ng of total protein in band 1, and thus detected submicrogram amounts of DHPR (Lamb et al., 1995).

Two Main Types of Cl$^-$ Channel Activity

Fusion of vesicles of bands 2, 3, and 4 introduced several kinds of Cl$^-$ channel into the bilayers. The channels were distinguished by their conductance, gating kinetics, sensitivity to SO_4^{2-}, and DIDS and voltage-dependence. Two types of channel were the most frequently incorporated and are described in this paper. The channels were identified as Cl$^-$ channels because the current reversed near the Cl$^-$ equilibrium potential and they were susceptible to block by several Cl$^-$ channel blockers including DIDS (see below). The first kind of channel gave currents with maximum unitary conductance of 210–250 pS, whereas the second had a maximum unitary conductance of 65–75 pS. For convenience, we have called them big (BCl) and small (SCl) Cl$^-$ channels. Each fusion event incorporated one to three Cl$^-$ channels into the bilayer that were either of the same type or a mixture of the two types. Recordings of multiple Cl$^-$ channels were not included in the analyses.

Fusion of band 1 vesicles into bilayers introduced two distinctly different types of chloride channel in addition to the channels seen in bands 2, 3, and 4. The channels specifically associated with band 1 (also occasionally seen–in <5% of incorporations–in bands 2 and 4) were not characterized in detail, but appeared similar to the 40 pS and 60 pS channels associated with plasmalemma and T-tubule membranes (see Table 1), in their conductance (<70 pS), and in the appearance of spontaneous channel openings at all membrane potentials. In one series of experiments, 7 of 9 channels incorporated from band 1 were non-voltage-dependent and similar to the plasmalemma/T-tubule channels (not typical SCl channels), and two channels were typical SCl channels.

BCl channels

The BCl channel was characterized by its high conductance and very high open probability at all bilayer potentials used. Because the channel seldom closed, it was often difficult to establish a baseline (closed) level. Incorporations of BCl channels into lipid bilayers were readily detected. During monitoring of bilayer capacitance (i.e., the "bilayer test"; see Materials and Methods) these channels always introduced a large conductive component into the bilayer impedance. This type of channel activity was seen in the bilayer in approximately one out of every two to three vesicle incorporations and was observed in 171 bilayers. An example of BCl channel activity is shown in Fig. 1 *B*, and the relationship between maximum current amplitude and holding potential is shown in Fig. 1 *D*. The relationship between current and voltage between −20 and +60 mV was approximately linear and the slope conductance within this range of potentials in Fig. 1 *D* was 245 pS. In seven BCl channels, the average slope conductance between −20 and +60 mV was 234 ± 6 pS. Analysis of continuous channel activity lasting for 2 to 4 minutes at 0 mV ($n = 7$) gave an average P_o of 0.97 ± 0.02 and an average mean current, I' (i.e., the integral of the current divided by the total time), of −7.7 ± 0.4 pA (compared with the maximum current of −9.7 pA at 0 mV calculated from the average slope conductance). Although not examined in detail here, we found that the P_o of BCl channels was high at all voltages between +60 mV and −60 mV.

The BCl channel was selective for Cl$^-$ ions. Solutions normally contained Cl$^-$ concentrations of 50 mM (*trans*) and 250 mM (*cis*) giving a Cl$^-$ equilibrium potential of about +40 mV (see Fig. 1 *D*). Solutions also contained Ca^{2+} at the same concentration (0.5 to 1 mM) on both sides of the membrane giving a calcium equilibrium potential of 0 mV. Because the reversal potential in 250/50 (*cis/trans*) choline Cl$^-$ was close to +40 mV (see, e.g., Fig. 1 *D*), the permeability for choline was negligible. The permeability ratio for Cs$^+$ to Cl$^-$ was ~0.03.

SCl channels

The second type of channel had a much lower conductance: the unitary current at 0 mV in Fig. 1 *C* was only about −3 pA, in contrast to about −10 pA in the BCl channel (Fig. 1 *B*). Our initial observation was that occasional SCl channel activity could be observed at +10 or 0 mV, but was usually not seen at −40 mV until the bilayer had been subjected to one or more voltage steps to positive potentials (+40 to +80 mV) for 1–2 s. Channel activity at +10 or 0 mV continued with a high P_o (>0.2) for several minutes after the voltage pulse before the channel became quieter, with long closed periods (lasting several seconds) separating spontaneous bursts of activity. In contrast, channel activity at −40 mV was maintained for only 5–30 s after the activating pulse before the channel became silent. The voltage-dependence of the SCl channel is considered in more detail later.

The current-voltage relationship for the SCl channel was also approximately linear between −20 and +40 mV (Fig. 1 *E*), but the slope conductance was much lower than that of the BCl channel. In Fig. 1 *E*, the slope conductance is 75 pS. In seven SCl channels, the average slope conductance was 68 ± 2 pS between −20 mV and +60 mV. The slope conductance decreased when Cl^- concentration decreased (three channels). In one channel, with 150, 100, and 50 mM *cis* Cl^-, the relative conductances were 86%, 69%, and 59% of the conductance in 250 mM *cis* Cl^-.

SCl channel activity was seen in approximately one out of every six to seven vesicle incorporations and was observed in 66 bilayers in this study. The average P_o within bursts of activity at 0 mV was 0.65 ± 0.10 and the average mean current, I' (i.e., the integral of the current divided by the total time), was −1.5 ± 0.3 pA ($n = 4$), compared with the maximum current of −2.7 pA at 0 mV (estimated from the average slope conductance).

The SCl channel was also selective for Cl^- ions. The reversal potential in 250/50 mM (*cis/trans*) choline Cl^- was close to +40 mV (see, e.g., Fig. 1 *E*), the Cl^- equilibrium potential. Furthermore, the mean reversal potentials of two channels in CsCl solutions 250/50 (*cis/trans*) was +36 ± 2 mV (errors estimated from linear regression of the data). The reversal potential changed to +25 ± 2 mV when CsCl on the *cis* side was reduced from 250 to 150 mM, and to +16 ± 2 mV when the *cis* CsCl was further reduced to 100 mM. These reversal potentials were 3 to 5 mV less than the Nernst potential for Cl^- ions and, when used in the Goldman, Hodgkin, and Katz equation, suggest that P_{Cs}/P_{Cl} was between 0.04 and 0.08. Under these conditions the SCl channel is highly selective for Cl^- ions over cesium ions.

Subconductance states and channel gating

General observations on subconductance states

Recordings of both BCl and SCl channels showed many current levels (Fig. 1, *B* and *C*). The gating of the BCl channel in particular appeared to be very complicated. BCl channels demonstrated several relatively long-lived (longer than 1 s) conductance levels that are apparent in Fig. 1 *B*. Fast "flickering" transitions to a myriad of intermediate conductance levels were maintained for several milliseconds and were seen as well as the long-lived levels. The flickering transitions can also be seen in Figs. 1 *B* and 2 *A*.

The BCl and SCl channel activity and the amplitude histograms shown in Fig. 2, *A* and *B*, illustrate the characteristic differences between the two channels. The records have been heavily filtered after sampling (see Fig. 2 legend) to display the conductance levels. The BCl channel is open mostly at levels near the maximum conductance. In contrast, the SCl channel is often open at levels below the maximum conductance. An initial indication of the conductance levels was obtained by visual examination of the data and of peaks in the amplitude histograms. Lines were drawn through the current records at the most obvious conductance levels (maintained >100 ms). Thirteen lines have been superimposed on the record of BCl channel activity in Fig. 2A, although there are clearly more levels that are maintained for shorter times. The 13 levels can also be seen as peaks in the amplitude histogram in Fig. 2 *A*.

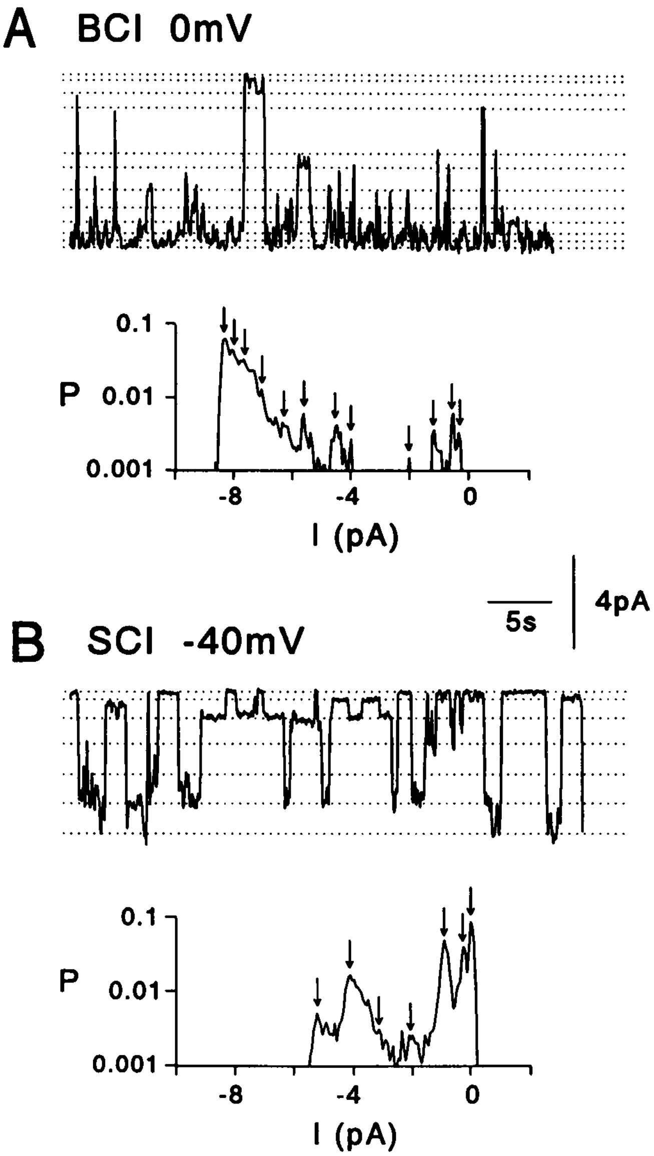

FIGURE 2 Multiple conductance levels in currents from BCl (*A*) and SCl (*B*) channels. The BCl channel activity was recorded at 0 mV and the SCl channel at −40 mV. Dotted lines have been drawn through levels maintained for >100 ms, which can be identified as peaks or humps in the all-points histograms. The uppermost level is the 0 current level. Data were heavily filtered to display conductance levels (moving average of 19 points). Arrows identify peaks or asymmetries on the all-points histograms that correspond to the levels indicated on the current records.

The pattern of SCl channel activity (Fig. 2 *B*) was very different from that of the BCl channel (Fig. 2 *A*). In contrast to the BCl channel, the SCl channel frequently closed to the zero current level and then opened to the maximum conductance. Several discrete conductance levels were apparent and were maintained for several hundred milliseconds in the heavily filtered data. The maximum conductance of this channel was 68 pS, i.e., the characteristic conductance of the SCl channel. The transitions between the zero current level and the maximum conductance (three examples can be seen in Fig. 2 *B*) indicate that the current passed through a single channel (see Discussion). Seven discrete conductance levels have been superimposed on the channel activity shown in Fig. 2 *B*. Some of these levels appear as peaks in the amplitude histogram in Fig. 2 *B*. The channel activities in Fig. 2, *A* and *B*, clearly show that there are a number of conductance levels in both BCl and SCl channels.

The records analyzed in Fig. 2 were heavily filtered, the allocation of levels was somewhat empirical, and the approach gave no information about the gating kinetics of the channel. Therefore the SCl and BCl channels were subjected to a more objective and quantitative analysis using two different analytical techniques, HMM and EVPROC.

Analytical techniques

Both HMM and EVPROC examine the data filtered at 1 kHz and use statistical techniques to extract the signal from the background noise. Descriptions of EVPROC and the HMM routines (A, B, and C), the derivation of amplitude histograms, and substate transitions are given in Materials and Methods. The two analysis techniques were employed because they use different assumptions to extract the idealized record. A comparison of the idealized signal estimated by the techniques can identify aspects of the signal that are either dependent on, or independent of, the underlying assumptions.

Characteristic traces for the BCl and SCl channels are shown in Fig. 3. Superimposed on these traces are the idealized signals given by HMM (routine C) and by EVPROC. HMM detected more of the brief, "flickering" transitions than EVPROC. The difference in the number of flickering transitions can be seen in the transition kinetics between the higher conductance levels of the SCl channel (Fig. 3, *C* and *D*).

Identification of the number and probability of conductance levels

The SCl channel. Histograms of amplitude probability for the SCl channel activity at 0 mV, generated by HMM and EVPROC analysis of 60 s segments of data (120,000 data points), are shown in Fig. 4, *A* and *B*. Sustained current levels in channel recordings can be identified by peaks in the amplitude histograms of the data.

The histogram obtained with HMM (routine A; 15 iterations, Fig. 4 *A*, solid line) showed fewer peaks than the histogram obtained with EVPROC (Fig. 4 *B*). Both techniques yield a more structured profile than the histogram of the raw data (Fig. 4 *A*, *broken line*). The number of peaks in the histogram obtained with EVPROC were more distinct when the contribution from sojourns shorter than 5 ms were excluded (Fig. 4 *B*, *solid line*). The peaks in the histogram including shorter events (Fig. 4 *B*, *broken line*) were broadened by the relatively large standard error on the amplitude of the short events (see Fig. 12, *A* and *B*, and Appendix). The peaks in the EVPROC histogram roughly correspond to peaks in the HMM histogram and to the seven most probable levels (see below) identified by HMM (Fig. 4 *B*, *vertical dotted lines*).

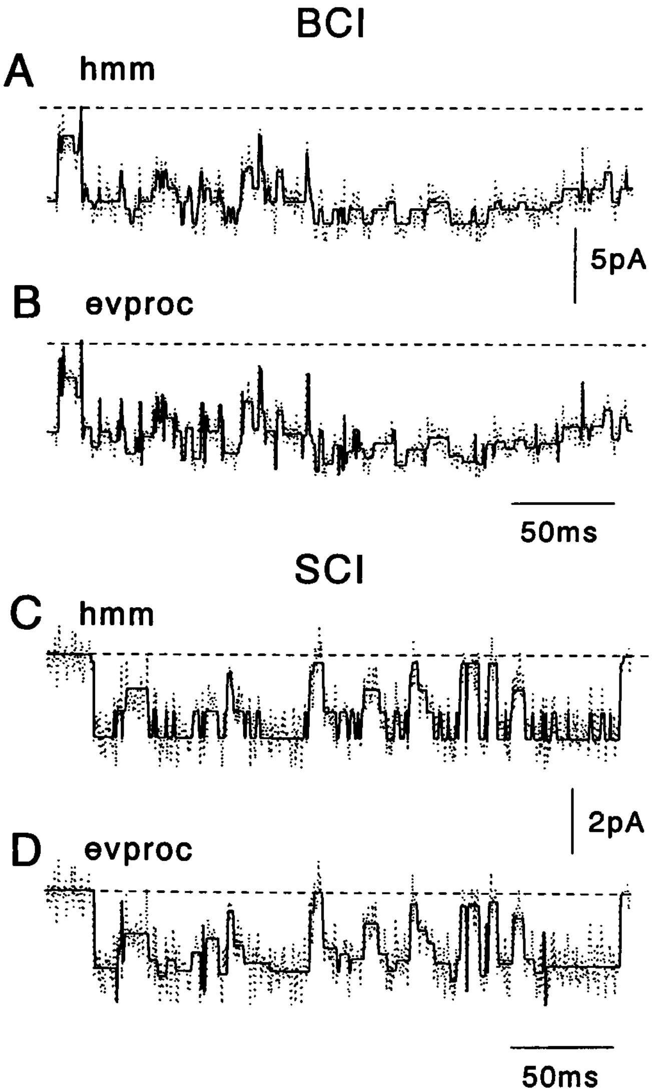

FIGURE 3 Detection of subconductance states in the BCl (*A* and *B*) and SCl channels (*C* and *D*) at 0 mV. 290 ms sections of records showing multiple conductance levels were selected and analyzed using HMM (hmm), routine C with 10 levels, and EVPROC (evproc); see Materials and Methods. Dotted lines are the current record, and solid lines are the current levels identified by the analysis techniques. Broken lines show the closed level. Note that a larger number of different levels are identified by both techniques for the BCl channel (*A* and *B*) than for the SCl channel (*C* and *D*). Data were filtered at 1 kHz and digitized at 2 kHz. The vertical calibrations are 5 pA for *A* and *B* and 2 pA for *C* and *D*. The horizontal calibration is 50 ms. Amplitude histograms and conductance levels obtained with EVPROC and HMM analysis of 60 s of data from the same channels are shown in Figs. 4, 5, and 6. Note that HMM identified 6 levels in this brief segment of data, and seven levels in the longer segment analyzed for Fig. 4 *A*, which contained some longer openings to the −3.6 pA level.

HMM (routine B) was used to look for the *n* most likely levels in the data. We found that the levels identified by

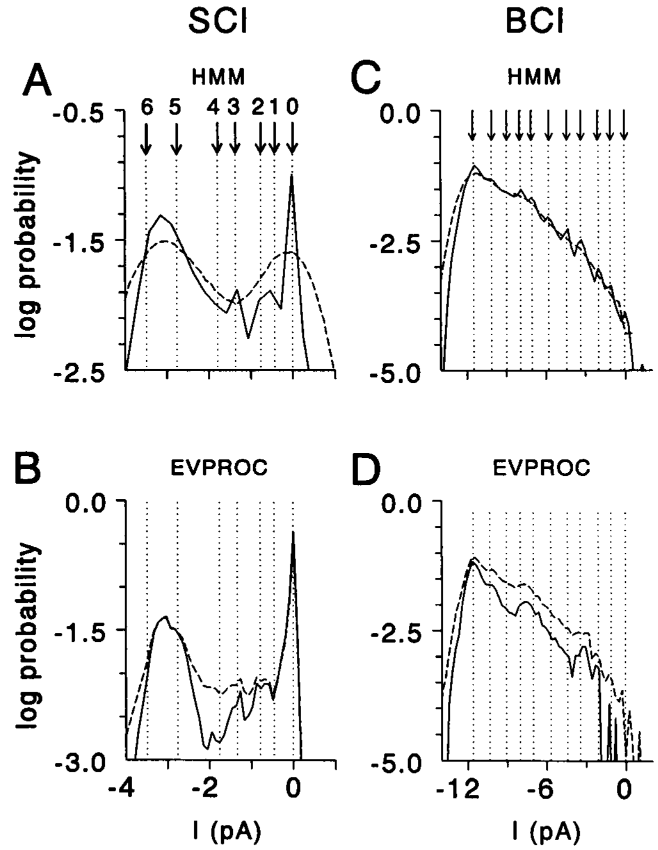

FIGURE 4 The probability of current amplitudes determined by EVPROC and HMM (routine A; see Materials and Methods) analysis of 60 s (120,000 data points) of channel activity from the SCl channel shown in Fig. 3, *C* and *D*, and the BCl channel shown in Fig. 3, *A* and *B*. (*A*) HMM analysis of the SCl channel. The level probabilities were produced by HMM after 15 iterations of routine A (with 24 levels; calculation time = 15 h on a SUN workstation (Sun SparcStation 2 operating system: SunOS 4.1.1)). Broken line shows the histogram for the raw data. Arrows and vertical dotted lines correspond to levels identified using HMM routine B. (*B*) EVPROC analysis of the SCl channel. Probability distributions were derived from normalized frequency distributions generated by EVPROC and show levels maintained for >1 ms (*dashed line*) or >5 ms (*solid line*). Vertical dotted lines indicate substate levels identified by HMM and are included for comparison. (*C*) HMM analysis of the BCl channel. Solid line shows level probabilities produced by HMM after 15 iterations of routine A (with 80 levels; calculation time = 6 days on the SUN workstation). Broken line shows the histogram for the raw data. Arrows and vertical dotted lines correspond to peaks in the histogram derived by HMM. (*D*) EVPROC analysis of the BCl channel. The probability distributions were derived as described for the SCl channel and show levels maintained for >1 ms (*dashed line*) or >5 ms (*solid line*). Vertical dotted lines indicate the peaks in the histogram derived by HMM and are included for comparison.

HMM increased with n up to a threshold value, n_t. When n was larger than n_t, additional levels formed tight clusters with other levels (i.e., grouped within 0.1 to 0.2 pA). The number of clusters did not appear to increase with further increases in n, and the likelihood of n levels did not increase significantly when $n > n_t$. Therefore we chose the number of clusters to represent the number of resolvable levels. The number of resolvable levels identified for the SCl channel varied from five to seven. The average conductance levels and probabilities for six channels are listed in Table 2. HMM consistently identified the closed state and two high conductance levels with high probabilities. Variations in the number of probable levels lay in variations in the number of low probability mid-conductance levels identified. The HMM analysis of the 60 s of SCl channel data in Fig. 3 yielded seven levels (Fig. 4 *A*) similar in number and conductance to the levels identified by eye in the heavily filtered record shown in Fig. 2 *B*.

Both HMM (routine A) and EVPROC histograms (Fig. 4, *A* and *B*) show 1) a broad peak centered at −3 pA, which appears to arise from the two closely spaced levels (dotted lines representing levels 5 and 6 at −3.5 and −2.8 pA obtained with HMM routine B); 2) a sharp peak representing the baseline (level 0) with a shoulder corresponding to a substate at −0.38 pA (level 1); and 3) several less distinct peaks between −0.5 and −2.5 pA (incorporating levels 3, 4, and 5).

The BCl channel. HMM (routine A) and EVPROC also produced fairly similar histograms of the amplitude probability for the BCl channel (Fig. 4, *C* and *D*). The histograms are sharply skewed toward the maximum current levels: the closed state was often not apparent in records lasting several minutes. The histograms from both analyses show multiple peaks separated by 1.1 ± 0.15 pA (mean ± SD). Dotted vertical lines have been drawn through the eleven peaks evident in the histogram derived by HMM (Fig. 4 *C*) and are superimposed on the EVPROC analysis in Fig. 4 *D*. Exclusion of shorter events from the EVPROC histograms shows these peaks more clearly (Fig. 4 *D*, *solid line*), although the baseline peak is seen only in the histogram which includes brief events (Fig. 4 *D*, *broken line*). On average, 10 ± 3 dominant peaks were distinguished by EVPROC from the "background" at 0 mV (seven channels) by their greater probability and their longer mean durations (see below). These dominant levels corresponded to the long-lived (see above) conductance levels that could be seen in the current records (e.g., see Fig. 1 *B*).

The approximately equal spacing of the 11 peaks in the histogram derived from HMM analysis (Fig. 4 *C*) raises the possibility that BCl channel activity originates from the gating of 10 25 pS channels (protochannels). The independence of these "protochannels" was tested by comparing the

TABLE 2 Average conductance levels identified by HMM in five SCl channels

γ (pS)	P
0	0.31 ± 0.09
5.0 ± 1.5	0.10 ± 0.05
15.5 ± 0.8	0.06 ± 0.02
28.7 ± 1.4	0.08 ± 0.02
49.8 ± 3.1	0.16 ± 0.02
68.2 ± 2.0	0.31 ± 0.03

The first column lists the average conductance (γ in (pS)). The second column lists the average probability of the current level (P) ± 1 SEM.

relative probabilities of the peaks with the binomial distribution expected for 10 independently gated, ~1 pA (25 pS) channels (not shown). It was found that the peak probabilities deviated significantly from the binomial distribution. The peak probabilities between 0 and −6 pA exceeded the binomial estimates by more than two orders of magnitude. This result indicated that, if the BCl channel has separately gated current paths, then the gating mechanisms must interact with each other.

Determination of the most probable levels using the available version of HMM (routine B) was limited because the software "looked" for, at most, 10 levels in the records. Consequently, the 10 most probable levels identified with routine B varied with time and were different for each channel analyzed. This is illustrated by the different levels in the BCl channels in Figs. 2, 3, and 4 *A*. In each case the 10 most probable levels identified by HMM would differ with variations in their relative probabilities. In general, HMM and EVPROC gave similar estimates of current levels and probabilities and were usefully employed together.

Records of BCl channel activity show many short-lived conductance levels (see above), indicating that the number of subconductance levels considerably exceeds 10 or 11. This was supported by HMM routine B analysis of three other BCl channels, which showed that the likelihood of n levels did not approach a maximum by $n = 10$, indicating that the number of subconductance states was >10 (Gage and Chung, 1994). In addition, a precedent for the number of levels exceeding the number of peaks is seen in the SCl channel where HMM routine B analysis yielded seven levels from data in which the histogram showed only four peaks (Fig. 4 *A*, above). Therefore the BCl channel might also contain more levels than the 11 peaks in the histogram in Fig. 4 *C*.

The kinetics of substate transitions

The SCl channel. HMM analysis of the SCl channel showed that the mean duration of open levels varied from 0.2 to 1.7 ms, and that the mean closed time was 10 ms (Fig. 5 *A*). The amplitude durations determined by EVPROC were three to five times longer than those determined by HMM, yet both analyses gave similar changes in durations over the range of amplitudes. The shorter durations determined by HMM reflected the higher transition detection rate of HMM than that of EVPROC (described with Fig. 3, above). The histograms obtained using EVPROC showed several peaks, some of which coincided with the seven levels identified by HMM in Fig. 4, *A* and *B* (shown as vertical dotted lines in Fig. 5, *A* and *B*).

Transition frequencies between conductance levels of the data analyzed in Fig. 5, *A* and *B*, were determined by EVPROC and HMM and are shown in 2-dimensional, gray-scale diagrams in Fig. 5, *C* and *D*. In these plots, the x axis shows the initial level, and the y axis shows the final level. Sample bins below the diagonal (Fig. 5, *C* and *D*) show the frequency of transitions from lower levels to higher levels, and sample bins above the diagonal show transitions from higher levels to lower levels. Both HMM and EVPROC identified frequent transitions between the levels in the high conductance range between −2.5 to −3.5 pA, shown by the black regions labeled *a* (Fig. 5, *C* and *D*). In addition, HMM (Fig. 5 *C*) revealed 1) frequent transitions between states near the baseline "b," 2) transitions between levels at −2.0

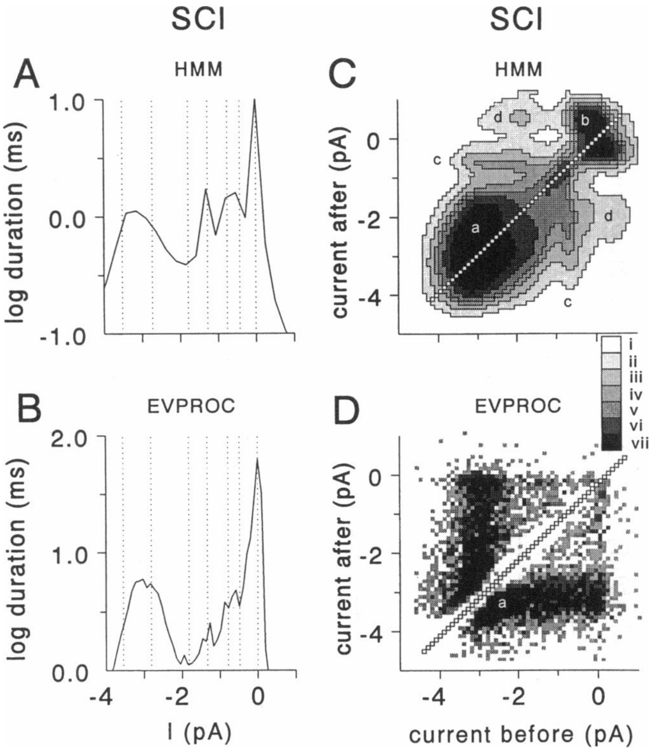

FIGURE 5 Gating kinetics of the SCl channel derived by HMM and EVPROC. *A* and *B* show the mean duration of all levels in the record. (*A*) Mean durations in the HMM analysis were calculated from the diagonal elements of the most likely signal transition matrix (see Materials and Methods), which was obtained from the analysis with routine A, described in the legend to Fig. 4 *A*. (*B*) Mean duration was derived from the EVPROC analysis by dividing the number of data points at each level by the number of events at each level. Vertical dotted lines in *A* and *B* indicate the substate levels identified by HMM in Fig. 4 *A* and are included for comparison. *C* and *D* show gray-scale diagrams of transitions between maintained current levels derived by HMM and EVPROC for the SCl channel. Squares (bins) below the diagonal (marked by connected diamonds) show the frequency of transitions to a larger (more negative) current amplitude, whereas points above the diagonal show transitions to a smaller (more positive) current amplitude. (*C*) SCl channel transition frequencies derived by HMM. The relative transition frequencies were derived from the signal transition matrix and have been scaled so that the range of transition frequencies is similar to that in Fig. 5 *D*. The dark region labeled *a* indicates a relatively high frequency of transitions between the higher conductance substates. There appear to be many transitions between levels near the baseline *b* and between levels at 2 pA and the baseline *c* and between substates in the −1 to −3 pA range and the substate at −0.8 pA *d*. (*D*) Transition frequencies produced by EVPROC. The dark region labeled *a* indicates a relatively high frequency of transitions between the higher conductance substates. The roman numerals beside the gray scale indicate the following numbers of transitions: i, 0–10; ii, 11–60; iii, 61–200; iv, 201–450; v, 451–900; vi, 901-1800; vii, 1800-∞.

and 0 pA "c," and 3) transitions from −0.8 pA to levels between −1 pA and −3 pA "d."

A comparison of the patterns generated by HMM and EVPROC reveals some differences in the way in which the analysis procedures interpreted the channel kinetics; the main difference was that EVPROC missed many transitions to midrange substates that occurred as the channel passed either from low to high, or from high to low, conductance levels. Thus EVPROC showed a higher frequency of large transitions that elongated the dark gray regions labeled *a* in Fig. 5 *D*, compared with region *a* obtained from HMM analysis (Fig. 5 *C*). The performance tests for EVPROC in the Appendix (see Fig. 12 *D*) indicate that, given the signal-to-noise ratio of the recording and the fast gating kinetics of the SCl channel, HMM is likely to give a more accurate picture of the gating kinetics.

The BCl channel. The mean duration of the BCl channel levels determined by HMM varied from 0.3 to 1.9 ms with closed times of 0.2 ms (Fig. 6 *A*). The EVPROC analysis yielded longer open times of 0.8 ms to 5.5 ms and a brief closed time of 0.68 ms (Fig. 6 *B*). Reasons for the longer event durations found by EVPROC have been discussed above. There are clearly many peaks in the histograms generated by both HMM and EVPROC. Some of the peaks correspond to peaks in the probability distributions for HMM in Fig. 4 *B* above (shown as dotted vertical lines in Fig. 6, *A* and *B*). As with the SCl channel, HMM and EVPROC gave qualitatively similar results, with the longest openings occurring at the higher conductance levels, relatively brief openings to lower conductance levels, and very brief closed times.

HMM and EVPROC yielded essentially identical patterns in transition diagrams for the BCl channel (Fig. 6, *C* and *D*). The transition diagrams indicate that most transitions are between nearby conductance levels and that most channel activity is between the higher conductance levels (Fig. 6, black areas labeled *a*). Very few large transitions (>4 pA) were detected, and the HMM analysis shows that some of the largest transitions (~6 pA) were between the midrange levels and levels near the baseline (areas labeled *b*).

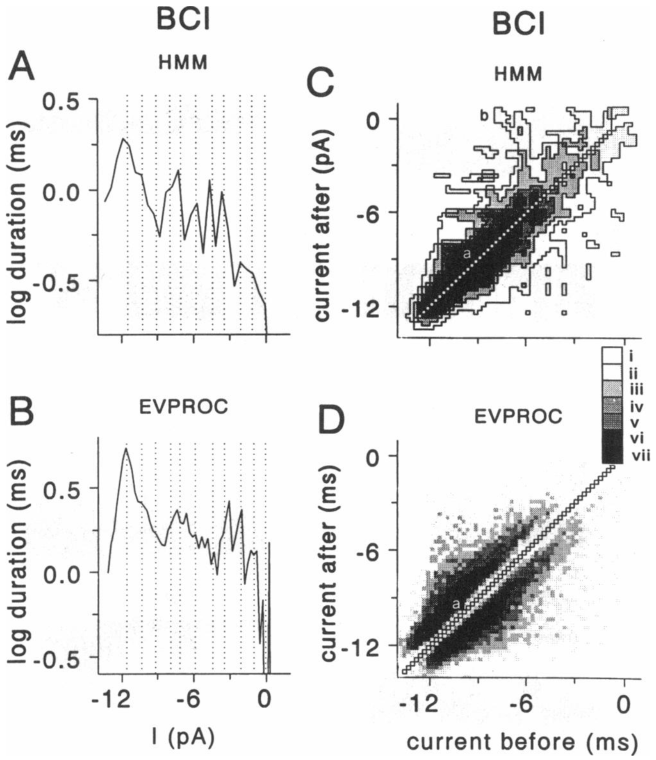

FIGURE 6 Gating kinetics of the BCl channel derived by HMM and EVPROC. *A* and *B* show the mean duration of all levels in the record, calculated in the same way as described for the SCl channel (see legend to Fig. 5). (*A*) Mean duration from HMM, calculated from the transition matrix from the analysis described in the legend to Fig. 4 *C*. (*B*) Mean duration from EVPROC analysis. Vertical dotted lines in *A* and *B* indicate the levels of peaks in the amplitude probability histograms derived by HMM for Fig. 4 *C* and are included for comparison. *C* and *D* show gray-scale diagrams of transitions between maintained current levels derived by HMM and EVPROC for the BCl channel. The axes and derivation of transitions are described in the legend to Fig. 5. (*C*) BCl channel transition frequencies derived by HMM. (*D*) BCl channel transition frequencies derived by EVPROC. The relative transition frequencies derived by EVPROC are similar to those derived by HMM. The black regions labeled *a* in *C* and *D* indicate that most transitions are between nearby high conductance substates. Some of the largest transitions (e.g., those labeled *b*) are between midrange levels and the lower substate levels. The roman numerals beside the gray scale indicate the following numbers of transitions: i, 0–10; ii, 11–60; iii, 61–200; iv, 201–450; v, 451–900; vi, 901–1800; vii, 1800–∞.

Distribution of BCl channels and SCl channels in SR vesicles

The BCl and SCl channels were found in both terminal cisternae (B4 vesicles) and longitudinal SR (B2 vesicles). Other types of Cl^- channel were seen infrequently and are not described here. The frequency of incorporation of Cl^- channels from B4 and B2 vesicles was indistinguishable. Of the single SCl + BCl channels obtained from B4 vesicles, ~76% were of the BCl type and 24% were SCl. Of single SCl + BCl channels in B2 vesicles, ~68% were BCl and 32% were SCl. The numbers of SCl channels were underestimated because bilayers were not always subjected to positive pulses. Both SCl and BCl channels were incorporated into bilayers at the same time as ryanodine-sensitive cation channels when B4 vesicles were used, suggesting an SR origin of both types of Cl^- channel. SCl and BCl channels were occasionally incorporated at the same time, suggesting that they are colocalized in the SR membrane.

Differential effects of sulfate

Addition of 30–70 mM Li_2SO_4 to the *cis* chamber reduced the amplitude of BCl channels as illustrated in Fig. 7 *A*. A small current of ~3 pA (75 pS) remained with occasional closures. A similar effect was seen with four of four BCl channels when these concentrations of sulfate were added to the *cis* chamber. Sulfate ions at the same concentrations had

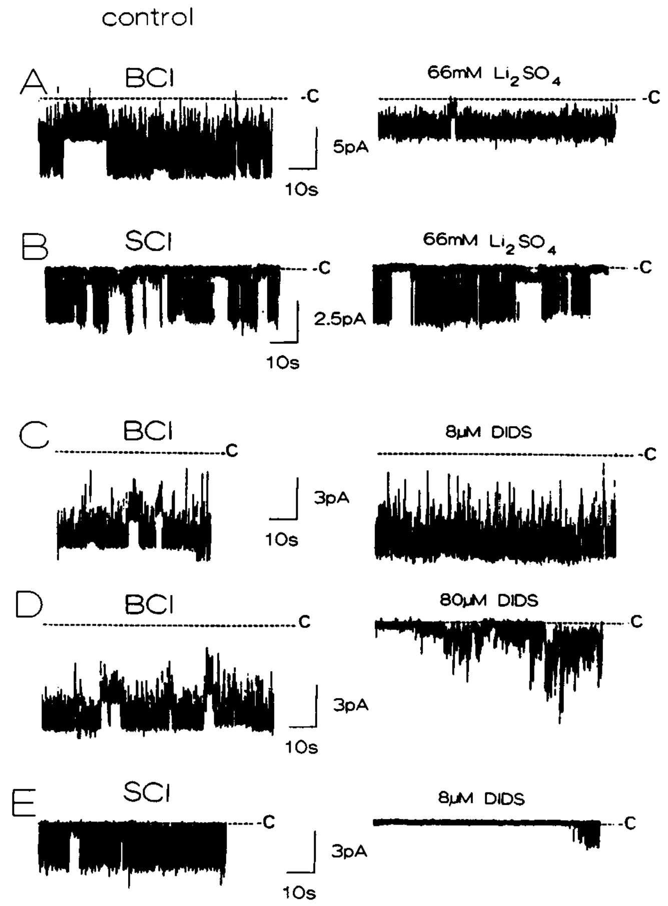

FIGURE 7 Effects of sulfate and DIDS on SR Cl$^-$ channels at 0 mV. *A* and *B* show a BCl channel and an SCl channel before (*left traces*) and after (*right traces*) addition of 66 mM Li$_2$SO$_4$ to the *cis* chamber. *C* and *D* show BCl channels before (*left panel*) and after (*right panels*), respectively, addition of 8 μM and 80 μM DIDS to the *cis* chamber. *E* shows an SCl channel before (*left panel*) and after (*right panel*) addition of 8 μM DIDS to the *cis* chamber.

no such effect on BCl channels when added to the *trans* chamber. Sulfate ions between 30 and 70 mM had no effect on SCl channels whether added to either the *cis* or the *trans* chamber (Fig. 7 *B*). Preliminary experiments (results not shown) suggest that the permeability of the channel to SO$_4^{2-}$ is similar to its permeability to Cl$^-$.

Differential effects of DIDS

DIDS at a concentration of 8 μM had no apparent effect on the BCl channel when added to either chamber (Fig. 7 *C*). At a much higher concentration (80 μM), DIDS decreased the open probability of channels (Fig. 7 *D*) whether added to the *cis* or *trans* chamber. In contrast to the effect of sulfate, large openings of the channel were still occasionally observed in the presence of 80 μM DIDS (Fig. 7 *D*). 80 μM DIDS added to the *cis* chamber reduced the open probability of the BCl channel in 21 out of 26 experiments, and when added to the *trans* chamber reduced the open probability in 7 out of 8 experiments.

SCl channels were more sensitive to DIDS than BCl channels. 8 μM DIDS markedly reduced the open probability and amplitude of SCl channels (Fig. 7 *E*) whether added to the *cis* (eight out of eight experiments) or *trans* chamber (two out of two experiments).

The voltage-dependence of SCl channels

The characteristic voltage-dependent activation, deactivation, and inactivation properties of the SCl channel in 250/50 CsCl can be seen in the single channel records in Fig. 8 *A* and in ensemble averages of activity from 12 to 17 channels in Fig. 8 *B*. The single channel records show that channel openings were brief and infrequent at +60 mV (Fig. 8 *A*). Bursts of activity were induced by steps in potential from +60 mV to 0 mV or to negative membrane potentials. The onset of activity became faster at more negative membrane potentials (Fig. 8 *B*). The mean latencies (time between the start of the pulse and the first channel opening) became shorter at more negative membrane potentials (Table 3), although latencies varied over a wide range (from 0 ms to several seconds) at most potentials. The time constant of the exponential fitted to the rising phase of the ensemble average current was clearly faster at more negative potentials (Fig. 8 *B*).

Another obvious potential-dependent phenomenon was the decay in open channel probability (Fig. 8 *A*), and in the ensemble current (Fig. 8 *B*), at more negative potentials. This phenomenon, which we have called "inactivation" by analogy with similar phenomena in voltage-activated channels (Hille, 1992), can be seen either as a cessation of single channel activity during the 10 s voltage steps to potentials between −40 mV to −100 mV (Fig. 8 *A*), or as a decay in the average ensemble current during pulses to −40 mV and −60 mV (Fig. 8 *B*). Clearly, inactivation occurred more rapidly at −60 mV than at −40 mV, and took several minutes at 0 mV (not shown). Exponentials fitted to the decay of the average current show the faster inactivation at more negative potentials (Fig. 8 *B*, Table 3). When the potential was returned to +60 mV, activity decayed (i.e., deactivation occurred) within 2–3 s (Fig. 8, *A* and *B*; Table 3). The results in Fig. 8 show why channel activity could not usually be recorded from channels incorporated into the bilayer at −40 mV until the bilayer was subjected to pulses to positive potentials. The channels became inactivated at −40 mV, and inactivation was removed (channels were "reprimed") during the pulses to positive potentials.

Analyses of channel activity (open probability, P_o; frequency of opening, F_o; mean open time, T_o) at different potentials, in 250/50 CsCl, were performed over four different durations to test for stationarity. The time periods examined were: 1) 0 to 0.75 or 1.0 s, 2) 0 to 1.5 or 2.0 s, 3) 0 to 10 s, and 4) 0 to 100 s. In each case the analysis period was equal to the length of the voltage pulse, except for the 2 s analysis, which was performed on the first 2 s of pulses lasting for 10 or 100 s.

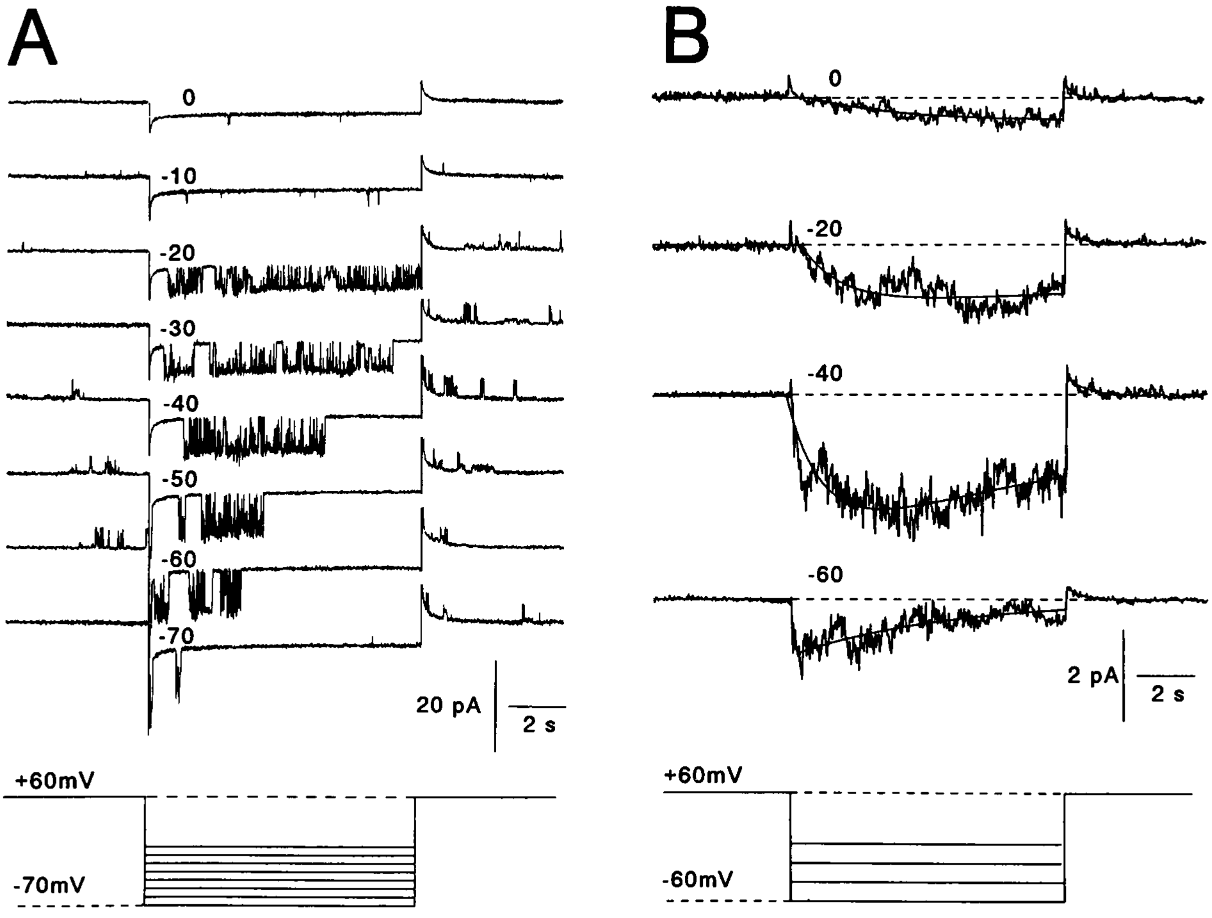

FIGURE 8 The voltage-dependence of SCl channel activity. (*A*) Family of single channel currents obtained using the voltage protocol shown beneath the records. A 10 s test pulse, applied from a holding potential of +60 mV, increased in 10 mV steps from +60 mV and −60 mV. The holding potential was maintained for 10 s between each test pulse. Current records between +60 mV and 0 mV contained little channel activity and are not shown. (*B*) Ensemble average currents constructed from data obtained from 12 to 17 channels. The transient capacitive currents were subtracted from each record before the ensemble average was constructed. Solid lines through the data show exponential curves fitted to the rise and decay of the current during the voltage pulse, and to the decay of activity when the bilayer potential was returned to +60 mV (see Table 3). The vertical calibration in *A* is current and in *B* is the mean current.

The average P_o, F_o, and T_o were independent of the duration of the measurement (0 to 0.75 or 100 s) for steps to potentials between +20 mV and −20 mV indicating that 1) the parameters of channel activity were stationary for up to 100 s after voltage steps to these potentials, and 2) there was no significant inactivation at periods up to 100 s after steps to potentials between +20 and −20 mV. Inactivation at potentials between −40 mV and −60 mV produced a reduction in P_o and F_o for the measurements made between 0 and 100 s, compared with measurements made at earlier times. The long latencies before the start of channel activity at potentials between +20 mV and −60 mV (Table 3, above) were expected to reduce the average P_o and F_o measured between 0 and 2 s, compared with measurements over longer times. However, this was not seen, possibly because of the large scatter in the average data and in latency values. There was no consistent difference between P_o, T_o, and F_o obtained between 0 and 0.75–1.0 s, and between 0 and 1.5–2.0 s. Therefore, these data were pooled and plotted as a function of membrane potential (Fig. 9).

P_o showed a bell-shaped voltage-dependence (Fig. 9 *A*). Average P_o was very low (<0.05) at potentials between +60 and +20 mV. A sudden increase in activity occurred at potentials between +10 and 0 mV, and the average P_o increased to a maximum of 0.5 at −40 mV and then decayed to values around 0.2 with steps to more negative potentials. The voltage-dependence of P_o was found to depend on changes in the frequency (F_o) and duration (T_o) of channel opening. A simultaneous increase in F_o (Fig. 9 *B*) and T_o (Fig. 9 *C*) between 0 and −40 mV produced the increase in P_o in this range of potentials. The fall in P_o between −40 and −100 mV was largely due to the reduction in T_o at more negative potentials, since the frequency of openings was constant (although the scatter was large) between −40 mV and −100 mV. The product of the curves fitted to average T_o and F_o provided a good fit to the P_o

TABLE 3 The effect of potential (*Vm*, first column) on minimal latency and the time constant (τ) of exponentials fitted to the rise and decay of the average ensemble currents shown in Fig. 6 *B*

Vm (mV)	Mean latency (ms)	τ_a (ms)	τ_i (ms)	τ_d (ms)
0	2271 ± 2524 (15)	3705	–	295.3
−20	808 ± 1413 (21)	1424	45,000	561.2
−40	431 ± 766 (29)	1352	15,712	725.7
−60	549 ± 1581 (41)	70.38	5723	478.4
−80	108 ± 139 (9)	–	–	–
−100	17 ± 10 (5)	–	–	–

Minimal latency was measured as the interval between the start of test voltage pulses and the first channel opening after the voltage step. The test voltage step was from a holding potential of +60 mV to potentials shown in the first column. The mean latency ± 1 SEM is given in the second column with the number of observations in parentheses below. The time constants of two exponentials fitted to average current during a test pulse, and an exponential fit to the decay in current after the test pulse, are given in columns 3–5. Column 3, time constant of the rise in the current amplitude during voltage pulses to negative potentials (time constant of activation, τ_a). Column 4, time constant of the decay in current amplitude during test voltage pulses to negative potentials (time constant of inactivation, τ_i). Column 5, time constant of the decay in current amplitude when the potential returns to the holding potential after a test pulse (time constant of deactivation, τ_d).

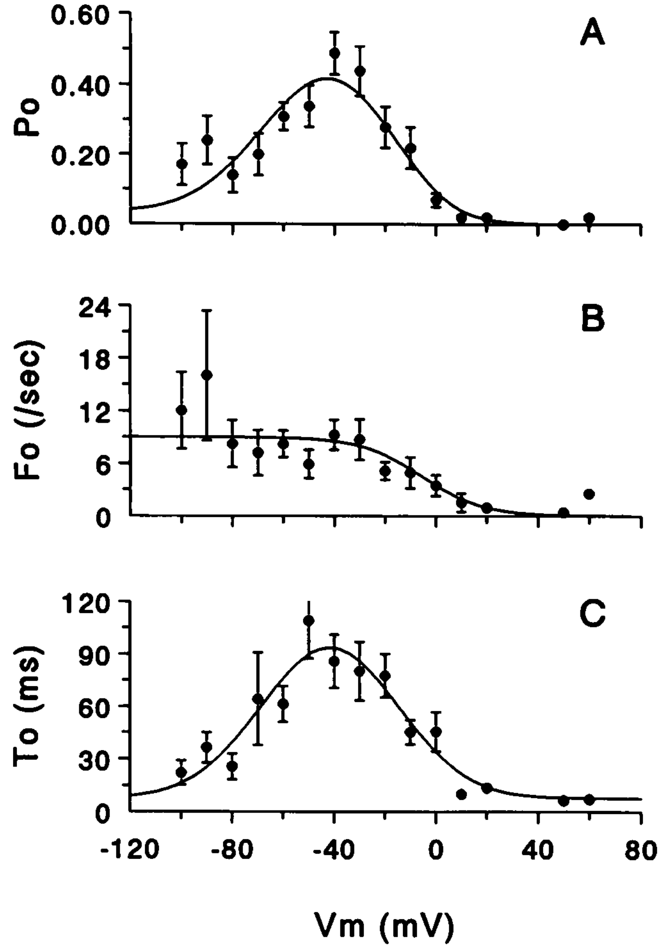

FIGURE 9 Analysis of channel activity within the first 2 s of voltage pulses from a holding potential of +60 mV to potentials (*Vm* (mV)) shown on the abscissa. Data at +60 mV was obtained at the holding potential between voltage pulses. (*A*) Open probability (P_o). (*B*) Frequency of channel opening (F_o). (*C*) Mean open time (T_o). The symbols show mean values of data from 12 to 17 single channels and the vertical bars indicate ± 1 SEM. Lines through the data in *B* and *C* are the best fits of a sigmoid and a Gaussian function, respectively. The curves of best fit have been multiplied and scaled to fit the data in *A*.

data. Therefore the voltage-dependence of P_o can be attributed to the voltage-dependence of F_o and T_o. Channel activation was examined in symmetrical 250/250 CsCl in one bilayer and the voltage-sensitivity was no different from that just described in 250/50 CsCl.

The bilayer potential appeared to have little effect on the distribution of closed times (between 0 and 1000 ms) measured during periods of activity (i.e., before inactivation), in marked contrast to the effect on open times. Two types of closed time histograms were constructed. In the first, histograms were first obtained for closures of <100 ms (few longer closures were observed between open events), using a bin width of 10 ms (Fig. 10 *A*). In all histograms for potentials between 0 mV and −100 mV, the data points for short closed times (<100 ms) appeared to be reasonably well fitted by a single exponential with a time constant of 4–5 ms (e.g., Fig. 10, *A* and *C*). However, three exponentials were found using a more sophisticated analysis. In the second type of histogram, the distributions of closed times (up to 1000 ms) were examined in plots of the square root of the frequency for log-binned closed durations (Sigworth and Sine, 1987). This technique allows greater resolution of infrequent events and revealed three exponential components in the closed times at each potential examined (Fig. 10 *B*, Table 4). The first two exponentials had time constants of ~3.0 ms and 22 ms. The longest component had values between 100 and 300 ms. Neither the time constants of the three components (Table 4), or their relative weightings (data not shown), appeared to be voltage-dependent.

The contribution from closed times longer than 30 ms to the closed time distributions (Fig. 10) was <10%; thus, "bursts" were defined as periods of activity in which closed times were <30 ms. An analysis of the characteristics of bursts of activity showed that the length of bursts was voltage-dependent. Average burst length was <100 ms at +10 mV and increased to a maximum of 400 ms at −60 mV, and then fell to ~200 ms between −70 mV and −100 mV (Fig. 11 *A*). The frequency of bursts was not voltage-dependent and was ~2/s between 0 mV and −100 mV (Fig. 11 *B*).

The voltage-dependence of steady-state inactivation (h_∞) was examined in preliminary experiments (n = 2). A 2 s test pulse to −70 mV was preceded by 10 s conditioning prepulses, which varied in 10 mV steps from +60 mV to −60 mV. A 5 s repriming period at +60 mV was allowed between conditioning pulses. The activity during the test pulse was reduced as the conditioning potential became more negative, so that activity was abolished after conditioning pulses to potentials of −30 mV and −40 mV.

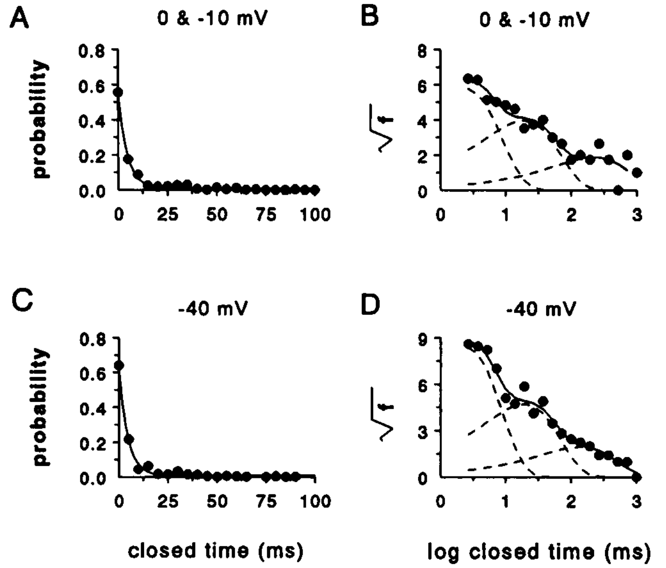

FIGURE 10 Effect of bilayer potential on channel closed times. Histograms constructed from data from 12 to 17 channels at 0–10 mV (*A* and *B*) and at −40 mV (*C* and *D*). *A* and *C* show data plotted linearly. Solid lines are single exponential curves fitted to the shorter closed times and had time constants of 4.5 ms (r^2 = 0.994) in *A* and 4.4 ms (r^2 = 0.992) in *C*. *B* and *D* show the square root of the frequency ($\sqrt{f}$) plotted using the log-bin method described by Sigworth and Sine (1987). Solid line shows the sum of the three exponentials fitted to the data, and the broken lines show the three exponential components. The time constants for the three exponentials in *B* and *D* are given in Table 6. There is very little difference between closed time histograms for 0–10 mV (where P_o is low) and −40 mV (where P_o is high). The data at 0 and 10 mV have been pooled to obtain a reasonable sample size.

Although there were insufficient data to construct an h_∞ curve with any confidence, these preliminary results show that the SCl channel is subject to a voltage-dependent inactivation process at negative potentials.

DISCUSSION

A novel voltage-activated Cl$^-$ channel in skeletal muscle SR vesicles

The results show that two types of Cl$^-$ channel are incorporated into bilayers with a high probability from mammalian skeletal muscle SR vesicles enriched in both longitudinal SR and terminal cisternae. The BCl channel is similar to the Cl$^-$ channel described by Tanifuji et al. (1987) in its ion selectivity (P_{Li}/P_{Cl} in the Tanifuji channel was 0.15), conductance, voltage-independent activity, and sensitivity to sulfate and DIDS. The SCl channel, on the other hand, appears to be a novel channel.

The SCl channel differs from previously described skeletal SR, plasmalemmal or T-tubule anion channels (Table 1) in that it displays steady-state inactivation only at negative potentials. The channels may not have been seen in previous studies because they are inactive when incorporated at negative potentials. Channel activity appeared at −40 mV immediately after pulses to positive potentials. This behavior is explained by the voltage-dependence of SCl channel activity. Channel openings were activated by voltage steps from a holding potential of +60 mV to negative potentials, and were deactivated on return to the holding potential. A slow decay in channel activity (inactivation) occurred during long (>2 s) pulses to negative potentials and recovery from inactivation occurred in 1–2 s when the potential was returned to +60 mV.

The properties of the SCl channel differ from properties previously described for skeletal SR channels in the following ways:

1) P_o of channels previously described from SR vesicles in bilayers is not voltage-dependent, and all channels show steady-state activation (Table 1).

2) In addition to differences in conductance (Table 1), the channel described by Rousseau et al. (1988) and Smith et al. (1986) differed from the SCl channel in that it was not completely blocked by DIDS even at millimolar concentrations and was blocked by 10 mM *cis* SO_4^{2-}. The SCl channel is blocked by μM DIDS, but not by SO_4^{2-}.

3) The 115 pS channel (Ide et al., 1991) was blocked by *cis* SO_4^{2-} (10 mM).

4) The 200 pS channel (Sukhareva et al., 1994) was not reported to be voltage-dependent and was blocked by 20 μM ruthenium red (the SCl channel is not blocked by 100 μM ruthenium red; J. I. Kourie, unpublished observations).

Channels that we observed infrequently in bands 2 and 4 may have corresponded to the lower conductance SR channel types described by others (Table 1) or may have been incorporated from contaminating plasmalemma or T-tubule membranes.

The conductance and voltage-dependence of the SCl channel is considerably lower than that of 500 pS Cl$^-$ channels in extruded blebs on the surface of skinned skeletal fibers (Table 1, nos. 9–10). Like mitochondrial voltage-dependent anion channels (VDAC, below) the channels were maximally active at 0 mV, and inactivated with voltage steps away from 0 mV. We see similar 500 pS channels (250/50 mM Cl$^-$) in bilayers after incorporation of solubilized SR proteins, and occasionally with incorporation of SR vesicles. The 500 pS channel may have been present in vesicles that did not readily fuse with the bilayers (Woodbury and Miller, 1990).

The SCl channel bears some resemblance to a voltage-dependent Cl$^-$ channel in cardiac SR (Rousseau, 1989). However, the cardiac Cl$^-$ channel exhibited a lower conductance than that of the SCl channel (Table 1) and steady-state activation. Furthermore, the cardiac channel activity was independent of [Ca^{2+}], in contrast to the SCl channel, which is Ca^{2+}-activated (Kourie et al., 1993). The SCl channel is surprisingly similar to Ca^{2+}-activated Cl$^-$ channel in endosomes from rat kidney cortex, which has a conductance of 90 pS in 150 mM KCl and a P_K/P_{Cl} of 0.08, is blocked by DIDS at μM concentrations, and has a voltage-dependent P_o that increases at negative potentials, with voltage-dependent inactivation at negative potentials (Reeves and Gurich, 1994).

TABLE 4 Effect of potential (*Vm*) on mean closed time

		τ		
Vm (mV)	A (ms)	B (ms)	C (ms)	D (ms)
0 and −10	42.8 ± 5.4 (271)	2.87 ± 0.85	22.5 ± 7.8	268 ± 179
−20	37.1 ± 7.0 (221)	3.25 ± 1.11	23.8 ± 23.1	105 ± 77
−40	21.3 ± 2.7 (450)	2.84 ± 0.41	22.7 ± 4.9	167 ± 76
−60	36.2 ± 4.9 (507)	3.11 ± 0.73	21.0 ± 5.4	317 ± 179
−80, −90, and −100	31.2 ± 3.8 (206)	3.21 ± 1.00	12.6 ± 3.1	316 ± 131

Mean closed times (mean ± 1 SEM with the number of observations in parentheses below) are shown in column A. The square root of frequency ($\sqrt{f}$) was plotted against the log-binned closed times (see text and Fig. 10 *B*). The sum of three exponentials was fitted to the data, and the time constants of the exponentials (τ) are given in columns B, C, and D. Too few closures were observed at +20 mV to construct reasonable histograms. Data at 0 mV and −10 mV have been lumped together, and data at −80 mV, −90 mV, and −100 mV, in order to obtain a reasonable number of observations to define the curves at these potentials. The time constant are given with ± 60% confidence limits for the fit to the data.

The properties of SCl channels differ from the properties of sarcolemmal and T-tubule channels in the following ways:

1) The high conductance sarcolemmal anion channels (Table 1, nos. 11–12) differ from the SCl channel in their conductance and in that they are not blocked by DIDS. Although P_o in the channel described by Woll and Neumcke (1987) was voltage-dependent, channel activity did not display the voltage-dependent activation and inactivation characteristics of the SCl channel. The channel described by Blatz and Magleby (1983), also like a VDAC (below), was active at 0 mV and inactivated after voltage steps away from 0 mV.

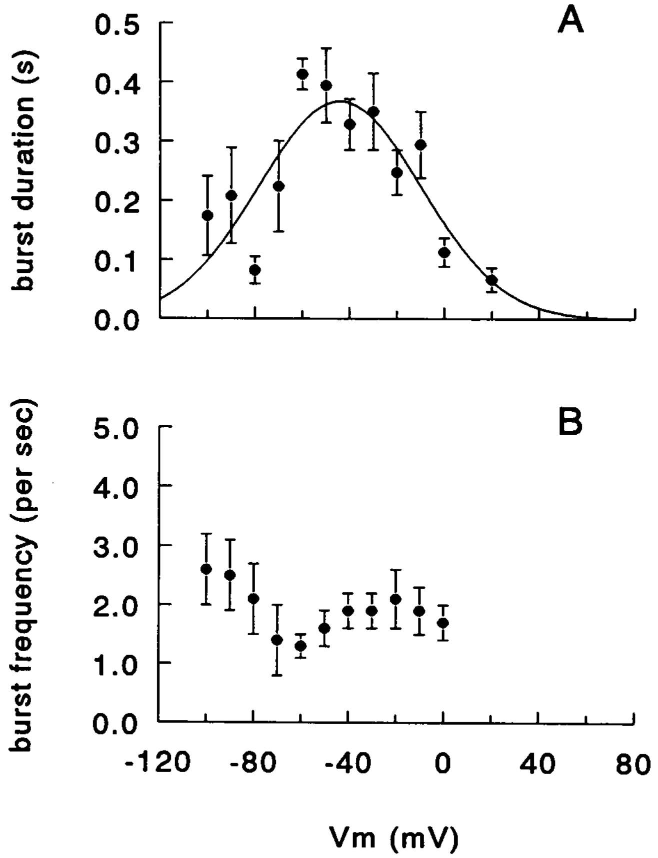

FIGURE 11 The dependence of burst activity on potential. (*A*) Burst duration (in seconds) plotted against potential (*Vm* (mV)). (*B*) Burst frequency (per second) plotted against potential. Bursts were defined as periods of activity separated by closed times longer than 30 ms, based on data shown in Fig. 10.

2) P_o of the smaller 40–60 pS anion channels in the sarcolemma (Table 1, nos. 14–16), like that of the SCl channel, is greater at −30 mV than at −80 mV. Unlike the SCl channel, these sarcolemmal channels remain active at all potentials.

3) In contrast to the SCl channel, neither the 35–280 pS channels seen in lipid supplemented vesicles (Table 1, nos. 13 and 18), nor the 40 pS T-tubule chloride channel (Table 1, no. 19), are voltage-dependent.

The properties of BCl channels differ from the properties of sarcolemmal and T-tubule channels in the following ways:

1) Two high conductance sarcolemmal anion channels with conductances comparable to that of the BCl channel are described by Woll and Neumcke (1987) and Blatz and Magleby (1983) (Table 1, nos. 11–12). P_o in both channels is strongly voltage-dependent, in contrast to P_o in the BCl channel which is essentially voltage-independent. In contrast to the BCl channel, the channel described by Woll and Neumcke (1987) is not blocked by DIDS and is only weakly anion-selective (P_{Na}/P_{Cl} of 0.25).

2) The 260 pS channel described by Wischmeyer et al. (1995) (Table 1, no. 13) is similar to the BCl channel in that it has a number of substates. However the strong rectification in the current-voltage relation of this channel is not seen with BCl channels.

The origin of SCl and BCl channels

We considered the possibility that the BCl and/or SCl channel might have come from mitochondrial, plasmalemmal, or T-tubule contamination of the SR vesicles. A mitochondrial origin seemed unlikely because neither channel had the same conductance or voltage-dependent gating seen in isolated VDAC from mitochondria. VDAC has a conductance of 700 pS, a high P_o over the range ±20 mV and switch to a low conductance, cation-selective state outside this range (Mirzabekov et al., 1993; Schein et al., 1976). In addition, the contamination of our B2 to B4 vesicles by mitochondrial outer membranes is <1% (estimated from monoamine oxidase activity; Junankar et al., 1995). Contamination with mitochondrial inner membrane is <3% (estimated from succinate cytochrome C reductase activity; S. M. Pace and P. R. Junankar, unpublished).

A plasmalemmal origin of SCl and BCl channels also seemed unlikely. The properties of the plasmalemma and T-tubule channels differ from those of the BCl and SCl channels (above). In addition, the SCl channel is found in all membrane fractions (B1 to B4), and SR membrane is present in significant and similar quantities in all fractions. Sarcolemmal membrane (Fig. 1), could be detected only in B1. The T-tubule membrane was 8–10 times greater in B1 than in B2 and 12–22 times greater in B1 than in B4. Had SCl channels arisen only from T-tubule membrane, we would have expected to see 8–10-fold more incorporation from B1 than B2, and 12–22-fold more incorporation from B1 than B4. These differences in incorporations were not seen.

The antibody to the SR Ca-ATPase may have cross-reacted with the T-tubule Ca-ATPase. However, this was unlikely to have contributed to estimates of relative amounts of SR membrane because 1) the density of Ca-ATPase in the T-tubule membrane is 1% of that in SR membrane; and 2) the T-tubule Ca-ATPase is ~140 kDa (C Hidalgo, personal communication), and an immunostaining band at 140 kDa was not seen.

Other evidence supporting the SR origin of BCl and SCl channels is that they were frequently incorporated into bilayers, apparently in the same fusion events as ryanodine-sensitive calcium channels found exclusively in SR. It is likely that the SCl and BCl channels were derived from the same membranes, given that both types of channel could be incorporated in the same fusion event. Although the evidence is strongly in favor of an SR origin for the SCl and BCl channels, the channels could arise from surface or T-tubule membranes if these membranes were preferentially incorporated into bilayers by a factor of 10-fold in B2 compared with B1 or 20-fold in B4 compared with B1. Alternatively, the channels might be expressed in SR, sarcolemma, and T-tubule membranes.

It is possible that an SR Cl^- channel arises from a VDAC-like protein. A VDAC (porin type 1) protein has been localized, using immunoelectron microscopy, in amphibian skeletal muscle SR (Lewis et al., 1994) and in plasmalemma and SR of mammalian skeletal and cardiac muscle (Junankar et al., 1995). VDAC protein is also expressed in extramitochondrial membranes of several other cell types (Jurgens et al., 1991; Thinnes, 1992; Puchelle et al., 1993). Because the single channel characteristics of the porins are likely to vary, depending on the membrane in which they are inserted (Thinnes, 1992), one or another of our Cl^- currents may arise from a VDAC protein. Antibodies to the VDAC (anti-porin 31L) have been shown, using immunoelectron microscopic techniques, to identify the VDAC protein in SR of rabbit muscle used to obtain vesicles for our channel studies and to immunostain a 31 kDa protein in all four bands of SR vesicles (Junankar et al., 1995).

Multiple conductance levels in BCl and SCl channels

Although the two analysis programs, HMM and EVPROC, used very different assumptions about the raw data in order to extract the idealized records, they gave a mostly consistent picture of the SCl and BCl channels' substate levels and transition kinetics. Both channels showed several conductance levels. The best resolution of substates by our analysis algorithms was achieved when the channel signal was filtered at 1 kHz. Naturally, the observed kinetics must depend on the bandwidth of the recording system. However, we found that the observed substate conductances did not appear to be sensitive to filtering. For example, HMM determination of substate levels for SCl channels recorded with a bandwidth of either 500 Hz or 1 kHz were not significantly different (not shown) and also matched levels that could be seen by the eye in more heavily filtered records.

The complex gating behavior of the BCl channel is a common property of large anion channels from a variety of sources (see e.g., Krouse et al., 1986). Because the putative single channel activity displayed more than two conductance states (open and closed), we needed to establish that the signal did not arise from the independent gating of multiple channels. Criteria used to distinguish between single and multiple channels have been reviewed by Fox (1987). A single channel with many conductance states may show transitions between non-adjacent current levels that are too frequent to result from coincident gating of independent channels, and these transitions have been used to identify single channels (Krouse et al., 1986). Most transitions of the SCl channel were between non-adjacent levels, so that it met the criterion for a single channel. In contrast to the SCl channel, BCl channel transitions were most often between adjacent conductance levels so that it was difficult to tell whether these were subconductance levels of one channel or the combined activity of several coupled or colocalized channels. However, it is unlikely that the BCl channel activity resulted from random incorporation of independent channels in the bilayer because it was always seen as a unit with a maximum conductance of 250 pS (see also Tanifuji et al., 1987). In addition, peaks in amplitude histograms deviated significantly from the binomial distribution, suggesting that the activity did not arise from independent channels. We are currently undertaking a more complete kinetic analysis and modeling of the gating kinetics of the BCl channel.

Voltage-dependent Cl^- channels

Voltage-dependent Cl^- channels have been described in the plasmalemma of several cell types. P_o of channels in skeletal muscle plasmalemma is usually higher at potentials positive to the resting membrane potential, than at the resting potential (Woll et al., 1987; Blatz and Magleby, 1985). P_o is bell-shaped with a maximum at 0 mV in one muscle plasmalemmal channel (Blatz and Magleby, 1983) and in VDAC in internal membranes of vertebrate cells (Schmid et al., 1988; Mirzabekov et al., 1993; Schein et al., 1976). In contrast to the vertebrate channels, a voltage-dependent Cl^- current in the algae, *Chara inflata*, is activated by hyperpolarization and counteracts changes in membrane potential induced by the H^+ pump (Tyerman et al., 1986; Kourie and Findlay, 1990). The gating of the SCl channel is similar to the Cl^- current in *C. inflata*, and unlike previously described voltage-dependent Cl^- channels in vertebrates, in that it is activated when the cytoplasmic potential becomes negative with respect to the SR lumen.

The role of Cl^- channels in the SR membrane

Cl^- channels in plasmalemma have a common role in stabilizing membrane potential (Hille, 1992). It is possible that Cl^- channels in the SR membrane are important in maintaining the SR membrane potential at, or near, 0 mV. There are no measurements of SR membrane potential during Ca^{2+} release and reuptake with a time resolution equivalent to that of the Ca^{2+} transient after a single action potential. Electron probe analysis and uptake of $[^{14}C]SCN^-$ (Somlyo et al., 1981; Ikemoto et al., 1994), suggest that the potential is 0 at rest. The myoplasm would tend to become positive with respect to the SR lumen during calcium release, and would tend to become negative during calcium reuptake. The Ca-ATPase in the SR exchanges one H^+ for one Ca^{2+} so that a potential as great as −50 mV develops in liposomes, in the absence of counter-ion channels (Yu et al., 1994).

Counter-ion flow during Ca^{2+} release and reuptake could occur through K^+ (Miller and Racker, 1976; Coronado et al., 1980; Wang and Best, 1994) or Cl^- channels in the SR membrane. Both K^+ and Cl^- appear to be necessary for optimal calcium regulation (Sukhareva et al., 1994; Ikemoto et al., 1994). However, assigning a specific functional significance to the K^+ channel, or to the BCl or SCl channel, is probably premature; in the intact SR, the channels may well have properties different from those that they demonstrate in sarcoballs or in bilayers. If BCl channels were open most of the time in the SR, it is difficult to understand why the SCl channel would be needed. Other large Cl^- channels, which also flicker rapidly between many conductance levels (Krouse et al., 1986), become active only many seconds after excision of a patch (P. W. Gage, unpublished observations) suggesting that they are modulated in situ by some cytoplasmic factor. Similar observations have been made with VDACs in the plasmalemma of astrocytes (Dermietzel et al., 1994). SR channels have not been recorded in vivo, and the BCl channel–and indeed all SR ion channels–may be regulated by myoplasmic factors.

If, however, the SCl channel in the SR has the voltage-dependence observed here, it would not be maximally active during release of Ca^{2+} from the SR when the myoplasm would be positive relative to the SR lumen. The SCl channel could play an important role in facilitating the recovery of SR Ca^{2+} by dissipating the negative myoplasmic potential produced by the calcium pump. The SR K^+ channel may not contribute significantly to counter-ion flow during Ca^{2+} release and accumulation into mammalian SR, since it is blocked by physiological Ca^{2+} and Mg^{2+} concentrations, and its P_o is very low at 0 mV and at negative potentials (Miller, 1978; Coronado et al., 1980). Indeed, blocking the SR K^+ channel (in the absence of Cl^- ions) leads to an increase in Ca^{2+} uptake and release, rather than the decrease that would be predicted if the channel provided a significant counter-current (Fink and Stephenson, 1987).

In conclusion, the results show that SR vesicles of rabbit skeletal muscle contain two common types of Cl^- channel. The BCl channel is similar to Cl^- channels previously described in the SR, whereas the SCl channel is a novel anion channel with voltage-dependent activation and inactivation characteristics.

APPENDIX

EVPROC performance

EVPROC was used to detect current transitions in multilevel recordings in this communication and in a previous paper (Laver, 1992). However, the performance of EVPROC in recovering idealized channel signals from noisy data has not been previously evaluated. The EVPROC algorithm was tested on computer-generated, "channel-like" signals produced by superimposing Gaussian, white noise on a known, periodic square-wave. Gaussian noise was derived from sequential averages of 10 random numbers generated by Microsoft-Quick Basic. The ability of EVPROC to recover the square-wave signal (i.e., "on time" = "off time") was measured for a range of signal periodicities (with cycles of between 4 and 240 data points) and over a range of amplitudes (the signal-to-RMS noise ratio, ranging from 0.75 to 6).

The all-points amplitude histogram of the noisy square-wave (0 to −3 pA) signal (signal-to-noise ratio = 1.5) before EVPROC analysis is shown in Fig. 12 *A* (*dotted line*). This distribution was independent of the signal period. The histogram for the raw data is compared with the all-points amplitude histograms compiled from the signal that was recovered by EVPROC for the cases when the original signal levels were sustained for either 120 data points (*solid line*) or 6 points (*dashed line*). Ideally, the amplitude histograms of the recovered signal should have equal, nonzero bin entries at the two signal stationary levels at 0 and −3 pA. The measurement limitations of the detection algorithm cause broadening of the distributions so that two peaks with approximately equal areas are observed in the histograms. Clearly, EVPROC is more effective at resolving transitions in long stationary levels (i.e., slow kinetics, 120 points) than brief signals (6 points). In the limit of high frequencies EVPROC does not detect any transitions but rather interprets the signal as a stationary level. The onset of this behavior can be seen as the central peak in the amplitude histograms of the brief six-point signal in Fig. 12 *A* (*dashed line*).

Fig. 12 *B* shows the normalized peak widths (SD′(peak), i.e., SD of the peaks/SD of the signal noise) of distributions such as that in Fig. 12 *A*, for signals having various level durations (N), plotted against $1/\sqrt{N}$. Ideally, the SD of these peaks should equal the SD of the background noise divided by the $\sqrt{N}$, which, in turn, is equal to the SEM of the signal in each level (Fig. 12 *B*, *solid line*). However, the ideal situation gives the best possible performance of the EVPROC algorithm in the limit of high signal-to-noise ratios. When the signal-to-noise ratio is <2 (e.g., 1.5, Fig. 12 *B*, *filled circles*) the amplitude resolution of EVPROC is significantly poorer than

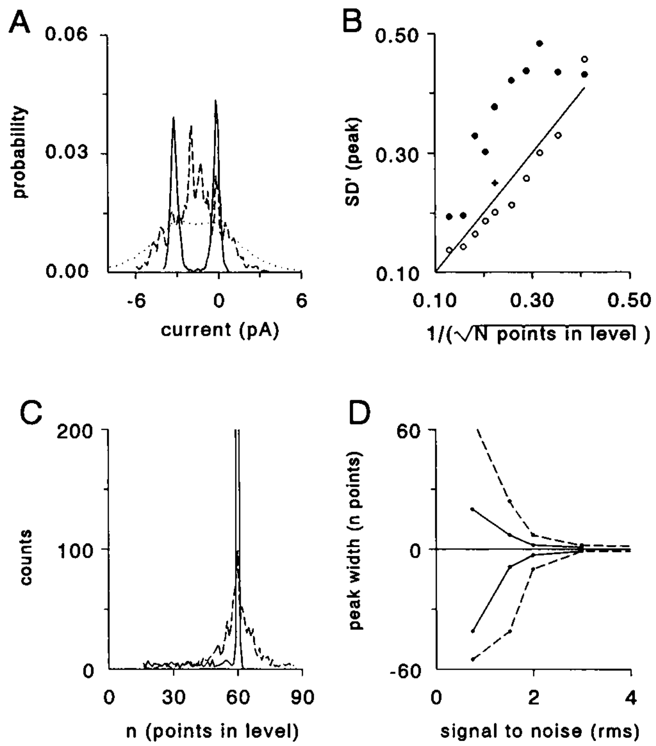

FIGURE 12 The performance of EVPROC in recovering "channel-like" square-wave signals from background noise. *A* and *B* show the ability of EVPROC to resolve levels of different amplitudes, and *C* and *D* show the temporal resolution of EVPROC. (*A*) A square wave (0 to −3 pA) was combined with white Gaussian noise (2 pA RMS) to produce a signal-to-noise ratio of 1.5. The amplitude probability histogram of the raw data (*dotted line*) is compared with histograms of the idealized record recovered using EVPROC. The amplitude histogram of the raw data is compiled from a square wave containing $N = 60$ points in each level. Amplitude histograms of signals recovered using EVPROC are shown for original signals having either 120 (*solid line*) or 6 (*dashed line*) points per level. It is clear that EVPROC peak distributions are sharper and the amplitude resolution better when the signal has long-lived levels. The dashed line shows the "breakdown" behavior of the EVPROC algorithm when the transitions between levels become too frequent for accurate level detection. The central peak in this distribution occurs because EVPROC interprets brief segments of the noisy square-wave as a single, half-amplitude level. (*B*) SD'(peak), the ratio of the standard deviation (SD) of the peaks in the amplitude histograms generated by EVPROC and the SD of the Gaussian noise on the signal, is plotted against the reciprocal of the square root of *N*, the number point in each level in the square wave. The results are shown for signals with signal-to-noise ratio of 1.5 (*filled circles*), 2 (*cross*) and 6 (*open circles*). The expected SEM of the data in each level, which represents the statistical limit to the performance of EVPROC, is shown by the solid line. (*C*) Frequency distribution of the number of points, *n*, in levels detected by EVPROC from a signal in which $N = 60$ and the signal-to-noise ratio was 1.5 (*dashed line*) or 6 (*solid line*). The distributions appear to have two distinct features: 1) a symmetric peak centred on $n = N$, with a width that appears to be independent of "*N*" (data not shown), and 2) a tail distribution extending down to $n = 0$, which is due to false triggerings of the EVPROC detection system by the background noise. The broader peak for lower signal-to-noise ratio indicates a poorer temporal resolution of the detection algorithm. (*D*) Dependence of the width of duration distributions, like those in *C*, on the signal-to-noise ratio. The peak widths are measured by the positive and negative confidence limits that bracket 67% (*solid line*) and 95% (*dashed line*) of the total counts. Further analysis (not shown) indicate that as a rule, EVPROC reliably recovers the durations of stationary levels that exceed the value of the 95% confidence limits. For example, if two current levels of a channel differ by 1 pA and the noise is 0.5 pA RMS (i.e., signal-to-noise ratio = 2) then the 95% confidence limits are ± 10 pA (see *C*), and EVPROC will reliably detect transitions between these levels if their durations are longer than ~10 data points.

the statistical limit. In this situation (i.e., a signal-to-noise ratio is <2), the errors in determining the exact times of signal transitions were found to introduce a significant component to the error in the level amplitudes.

The temporal accuracy of the EVPROC algorithm was measured from frequency distributions of level durations compiled from the recovered signals. Fig. 12 *C* shows distributions obtained from a signal with 60 points per level and with signal-to-noise ratio of either 6 (Fig. 12 *C*, *broken line*) or 1.5 (*solid line*). Ideally these frequency distributions should only have nonzero entries for bins containing durations of 60 points. The spread in the peaks arises from the uncertainty in determining the time of the current transitions. The uncertainty increases as the signal-to-noise ratio gets smaller but does not depend on the level duration (not shown). In a separate analysis EVPROC appeared to reliably recover the signal kinetics provided the level durations in the underlying signal exceeded the 95% confidence limits of the peak frequency distributions. Fig. 12 *D* shows the relationship between these confidence limits and the signal-to-noise ratio (67%, *thick line*; 95%, *thin line*, Fig. 12 *D*). It can be seen from the confidence limits in Fig. 12 *D* that the peak widths dramatically increase when the signal-to-noise ratio becomes <2.

These tests indicate that EVPROC is useful for analyzing multilevel channel recordings in which most current transitions exceed double the RMS noise level or where the channel gating is relatively slow. We found that a major advantage of EVPROC is that the calculations are fast so that the algorithm is well suited for analyzing long recordings from channels that may exhibit substates only rarely.

The authors are indebted to the John Curtin School of Medical Research workshops, in particular Bernie Keys, Graham Morgan, Bill O'Hare, and Nick Best. We are also grateful to Suzie Pace for isolating and characterizing SR vesicle preparations and preparing Western blots of vesicle proteins, to Michael Smith for assistance with programming, to Lin Roden and Joan Stivala for assistance, and to S. C. Froehner for providing us with the monoclonal antibody to the α_1 subunit of the DHPR. D. R. L. is an Australian Research Council Senior Research Fellow.

REFERENCES

Ahern, G. P., P. R. Junankar, and A. F. Dulhunty. 1994. Single channel activity of the ryanodine receptor calcium release channel is modulated by FK506. *FEBS Lett.* 352:369–374.

Blatz, A. L., and K. L. Magleby. 1983. Single voltage-dependent chloride-selective channels of large conductance in cultured rat muscle. *Biophys. J.* 43:237–241.

Blatz, A. L., and K. L. Magleby. 1985. Single chloride-selective channels active at resting membrane potentials in cultured rat skeletal muscle. *Biophys. J.* 47:119–123.

Chua, M., and W. J. Betz. 1991. Characterization of ion channels on the surface membrane of adult rat skeletal muscle. *Biophys. J.* 59: 1251–1260.

Chung, S. H., J. B. Moore, L. Xia, L. S. Premkumar, and P. W. Gage. 1990. Characterization of single channel currents using digital signal processing techniques based on Hidden Markov Models. *Philos. Trans. R. Soc. Lond. (Biol.)* 329:265–285.

Coronado, R., R. L. Rosenberg, and C. Miller. 1980. Ionic selectivity, saturation, and block in a K^+-selective channel from sarcoplasmic reticulum. *J. Gen. Physiol.* 76:425–446.

Dermietzel, R., T. -K. Hwang, R. Buettner, A. Hofer, E. Dotzler, M. Kremer, R. Deutzmann, F. P. Thinnes, G. I. Fishman, D. C. Spray, and D. Siemen. 1994. Cloning and *in situ* localization of a brain-derived porin that constitutes a large-conductance anion channel in astrocytic plasma membranes. *Proc. Natl. Acad. Sci. USA.* 91:499–503.

Dulhunty, A. F. 1979. Distribution of potassium and chloride permeability over the surface and T-tubule membranes of mammalian skeletal muscle. *J. Membr. Biol.* 45:293–310.

Dulhunty, A. F., M. R. C. Banyard, and C. J. Medveczky. 1987. Distribution of calcium ATPase in the sarcoplasmic reticulum of fast- and slow-twitch muscles determined with monoclonal antibodies. *J. Membr. Biol.* 99:79–92.

Dulhunty, A. F., P. R. Junankar, and C. Stanhope. 1992. Extrajunctional ryanodine receptors in the terminal cisternae of mammalian skeletal muscle fibres. *Proc. R. Soc. Lond. B Biol. Sci.* 247:69–75.

Eisenberg, R. S., and P. W. Gage. 1969. Ionic conductances of the surface and transverse tubular membranes of frog sartorius fibers. *J. Gen. Physiol.* 53:279–297.

Fink, R. H. A., and D. G. Stephenson. 1987. Ca^{++}-movements in muscle modulated by the state of K^+-channels in the sarcoplamic reticulum membranes. *Pflugers Arch.* 409:374–380.

Fox, J. A. 1987. Ion channel subconductance states. *J. Membr. Biol.* 97:1–8.

Gage, P. W., and S. -H. Chung. 1994. Influence of membrane potential on conductance sublevels of chloride channels activated by GABA. *Proc. R. Soc. Lond. B Biol. Sci.* 255:167–172.

Gurnett, C. A., S. D. Kahl, R. D. Anderson, and K. P. Campbell. 1995. Absence of the skeletal muscle sarcolemma chloride channel C1C-1 in myotonic mice. *J. Biol. Chem.* 270:9035–9038.

Hals, G. D., P. G. Stein, and P. T. Palade. 1989. Single channel characteristics of a high conductance anion channel in "sarcoballs". *J. Gen. Physiol.* 93:385–410.

Hamilton, S. L., R. M. Alvarez, M. Fill, M. J. Hawkes, K. L. Brush, W. P. Schilling, and E. Stefani. 1989. [3H]PN200-110 and [3H]ryanodine binding and reconstitution of ion channel activity with skeletal muscle membranes. *Anal. Biochem.* 183:31–41.

Hidaka, J., T. Ide, T. Kawasaki, T. Taguchi, and M. Kasai. 1993. Characterisation of a Cl^--channel from rabbit transverse tubules in the planar lipid bilayer system. *Biochem. Biophys. Res. Commun.* 191:977–982.

Hille, B. 1992. Ionic channels of excitable membranes. Sinauer Assoc. Inc., Sunderland, MA.

Ide, T., H. Sakamoto, T. Morita, T. Taguchi, and M. Kasai. 1991. Purification of a Cl^--channel protein of sarcoplasmic reticulum by assaying the channel activity in the planar lipid bilayer system. *Biochem. Biophys. Res. Commun.* 176:38–44.

Ikemoto, N., M. Yano, R. El-Hayek, B. Antoniu, and M. Morii. 1994. Chemical depolarization-induced SR calcium release in triads isolated from rabbit skeletal muscle. *Biochemistry.* 33:10961–10968.

Junankar, P. R., A. F. Dulhunty, S. M. Curtis, S. M. Pace, and F. P. Thinnes. 1995. Porin-Type 1 proteins in plasmalemma and sarcoplasmic reticulum of striated muscle fibres. *J. Muscle Res. Cell Motil.* 16(6).

Jurgens, L., P. Ilsemann, H. D. Kratzin, D. Hesse, K. Eckart, F. P. Thinnes, and N. Hilschmann. 1991. The primary structures of "Porin 31HM" purified from human skeletal muscle membranes and of "Porin 31HL" derived from human B lymphocyte membranes are identical. *Biol. Chem. Hoppe Seyler.* 372:455–463.

Kourie, J. I. 1995. Effects of the vagaries of block lipid membranes on characteristics of the SC1 channel from the sarcoplasmic reticulum of skeletal muscle. *Proc. Aust. Physiol. Pharmacol. Soc.* 26:120.

Kourie, J. I., and G. P. Findlay. 1990. Ionic currents across the plasmalemma of *Chara inflata* cells. *J. Exp. Bot.* 41:151–163.

Kourie, J. I., D. Laver, P. R. Junankar, A. F. Dulhunty, and P. W. Gage. 1992. Characteristics of chloride channels from longitudinal sarcoplasmic reticulum and terminal cisternae of skeletal muscle incorporated into artificial planar bilayers. *Proc. Aust. Physiol. Pharmacol. Soc.* 23:201.

Kourie, J. I., D. R. Laver, A. Premkumar, P. R. Junankar, and A. F. Dulhunty. 1993. The calcium-activation of a voltage-dependent chloride channel from the sarcoplasmic reticulum of skeletal muscle. *Proc. Aust. Physiol. Pharmacol. Soc.* 24:138.

Krouse, M. E., G. T. Schneider, and P. W. Gage. 1986. A large anion-selective channel has seven conductance levels. *Nature.* 319:58–60.

Lamb, G. D., P. R. Junankar, and D. G. Stephenson. 1995. Raised intracellular $[Ca^{++}]$ abolishes excitation-contraction coupling in skeletal muscle fibres of rat and toad. *J. Physiol.* In press.

Laver, D. R. 1992. Divalent cation block and competition between divalent and monovalent cations in the large conductance K^+ channel from *Chara australis. J. Gen. Physiol.* 100:269–300.

Laver, D. R., L. D. Roden, G. P. Ahern, K. R. Eager, P. R. Junankar, and A. F. Dulhunty. 1995. Cytoplasmic Ca^{++} inhibits the ryanodine receptor from cardiac muscle. *J. Membr. Biol.* 47:7–22.

Lewis, T. M., A. F. Dulhunty, P. R. Junankar, and C. Stanhope. 1992. Ultrastructure of sarcoballs on the surface of skinned amphibian skeletal muscle fibres. *J. Muscle Res. Cell Motil.* 13:640–653.

Lewis, T. M., M. L. Roberts, and A. H. Bretag. 1994. Immunolabelling for VDAC, the mitochondrial voltage-dependent anion channel, on sarcoplasmic reticulum from amphibian skeletal muscle. *Neurosci. Lett.* 181: 83–86.

Miller, C. 1978. Voltage-gated cation conductance channel from fragmented sarcoplasmic reticulum: steady-state electrical properties. *J. Membr. Biol.* 40:1–23.

Miller, C., and E. Racker. 1976. Ca^{++}-induced fusion of fragmented sarcoplasmic reticulum with artificial planar bilayers. *J. Membr. Biol.* 30:283–300.

Mirzabekov, T., C. Ballarin, M. Nicolini, P. Zatta, and M. Catia Sorgato. 1993. Reconstitution of the native mitochondrial outer membrane in planar bilayers. Comparison with the outer membrane in a patch pipette and effect of aluminium compounds. *J. Membr. Biol.* 133:129–143.

Mitchell, R. D., P. Palade, and S. Fleischer. 1983. Purification of morphologically intact triad structures from skeletal muscle. *J. Cell Biol.* 96: 1008–1016.

Morton, M. E., and S. C. Froehner. 1987. Monoclonal antibody identifies a 200-kDa subunit of the dihydropyridine-sensitive calcium channel. *J. Biol. Chem.* 262:11904–11907.

Palade, P. T., and R. L. Barchi. 1977. Characteristics of the chloride conductance in muscle fibers of the rat diaphragm. *J. Gen. Physiol.* 69:325–342.

Puchelle, E., J. Jacquot, C. Fuchey, H. Burlet, J. -M. Klossek, L. Gilain, J. -M. Triglia, F. P. Thinnes, and N. Hilschmann. 1993. Immunolocalization of porin and CFTR channels in human surface respiratory epithelium. *Biol. Chem. Hoppe Seyler.* 374:297–304.

Pusch, M., K. Steinmeyer, and T. J. Jentsch. 1994. Low single channel conductance of the major skeletal muscle chloride channel, ClC-1. *Biophys. J.* 66:149–152.

Reeves, W. B., and R. W. Gurich. 1994. Calcium-dependent chloride channels in endosomes from rabbit kidney cortex. *Am. J. Physiol.* 266:C741–C750.

Rousseau, E. 1989. Single chloride-selective channel from cardiac sarcoplasmic reticulum studied in planar lipid bilayers. *J. Membr. Biol.* 110:39–47.

Rousseau, E., M. Roberson, and G. Meissner. 1988. Properties of single chloride selective channel from sarcoplasmic reticulum. *Eur. Biophys. J.* 16:143–151.

Saito, A., S. Seiler, A. Chu, and S. Fleischer. 1984. Preparation and morphology of sarcoplasmic reticulum terminal cisternae from rabbit skeletal muscle. *J. Cell Biol.* 99:875–885.

Schein, S. J., M. Colombini, and A. Finkelstein. 1976. Reconstitution in planar lipid bilayers of a voltage-dependent anion-selective channel obtained from paramecium mitochondria. *J. Membr. Biol.* 30:99–120.

Schmid, A., H. Gogelein, T. P. Kemmer, and I. Schulz. 1988. Anion channels in giant liposomes made of endoplasmic reticulum vesicles from rat exocrine pancreas. *J. Membr. Biol.* 104:275–282.

Sigworth, F. J., and S. M. Sine. 1987. Data transformations for improved display and fitting of single-channel dwell time histograms. *Biophys. J.* 52:1047–1054.

Smith, J. S., R. Coronado, and G. Meissner. 1985. Sarcoplasmic reticulum contains adenine nucleotide-activated calcium channels. *Nature.* 316: 446–449.

Smith, J. S., R. Coronado, and G. Meissner. 1986. Single-channel calcium and barium currents of large and small conductance from sarcoplasmic reticulum. *Biophys. J.* 50:921–928.

Somlyo, A. V., H. Gonzalez-Serratos, H. Shuman, G. McClellan, and A. P. Somlyo. 1981. Calcium release and ionic changes in the sarcoplasmic reticulum of tetanized muscle: An electron-probe study. *J. Cell Biol.* 90:577–594.

Sukhareva, M., J. Morrissette, and R. Coronado. 1994. Mechanism of chloride-dependent release of Ca^{++} in the sarcoplasmic reticulum of rabbit skeletal muscle. *Biophys. J.* 67:751–765.

Tanifuji, M., M. Sokabe, and M. Kasai. 1987. An anion channel of sarcoplasmic reticulum incorporated into planar lipid bilayers: single-channel behavior and conductance properties. *J. Membr. Biol.* 99: 103–111.

Thinnes, F. P. 1992. Evidence for extra-mitochondrial localization of the VDAC/Porin channel in eucaryotic cells. *J. Bioenerg. Biomembr.* 24: 71–75.

Tyerman, S. D., G. P. Findlay, and G. J. Paterson. 1986. Inward membrane current in *Chara inflata*. II. Effects of pH, Cl^--channel blockers and NH_4^+, and significance for the hyperpolarized state. *J. Membr. Biol.* 89:153–161.

Vivaudou, M. B., J. J. Singer, and J. V. Walsh. 1986. An automated technique for analysis of current transitions in multilevel single-channel recordings. *Pflugers Arch.* 407:355–364.

Wang, J., and P. M. Best. 1994. Characterization of the potassium channel from frog skeletal muscle sarcoplasmic reticulum membrane. *J. Physiol.* 477:279–290.

Wischmeyer, E., S. Weber-Schurholz, and H. Jockusch. 1995. Sarcolemmal chloride and potassium channels from normal and myotonic mouse muscle studied in lipid supplemented vesicles. *Biochem. Biophys. Res. Commun.* 213:513–518.

Woll, K. H., M. D. Leibowitz, B. Neumcke, and B. Hille. 1987. A high-conductance anion channel in adult amphibian skeletal muscle. *Pflugers Arch.* 410:632–640.

Woll, K. H., and B. Neumcke. 1987. Conductance properties and voltage dependence of an anion channel in amphibian skeletal muscle. *Pflugers Arch.* 410:641–647.

Woodbury, D. J., and C. Miller. 1990. Nystatin-induced liposome fusion. *Biophys. J.* 58:833–839.

Yu, X., L. Hao, and G. Inesi. 1994. A pK change of acidic residues contributes to cation countertransport in the Ca-ATPase of sarcoplasmic reticulum. *J. Biol. Chem.* 269:16656–16661.